# Multi-decadal variations in delta shorelines and their relationship to river sediment supply: An assessment and review

Manon Besset, Edward J. Anthony, Frederic Bouchette

**HAL Id: hal-02190174**
**https://hal.umontpellier.fr/hal-02190174**

Submitted on 22 Oct 2021

# Multi-decadal variations in delta shorelines and their relationship to river sediment supply: An assessment and review

Manon Besset[a,b,*], Edward J. Anthony[b,c], Frédéric Bouchette[a]

[a]*Montpellier Univ, Geosciences Montpellier, UMR 5243, Montpellier, France*
[b]*Aix Marseille Univ, CNRS, IRD, INRA, Coll France, CEREGE, Aix-en-Provence, France*
[c]*CNRS, UG, IFREMER, LEEISA USR 3456, Centre de recherche de Montabo, Cayenne, Guyane française*

# Abstract

The inception, growth, and decline of numerous large and small river deltas on Earth have been strongly influenced by human population dynamics and interventions on catchments, notably deforestation and reforestation. Over the last half century, the effects of catchment conditions in determining fluvial sediment supply have been exacerbated or moderated by dams and reservoirs. The sediment balance of river deltas, crucial in terms of delta shoreline stability, advance or retreat, and subsidence, has, in turn, been affected by variations in fluvial sediment supply. The shoreline mobility and resulting subaerial coastal area changes of a selection of 54 of the world's deltas was quantified over 30 years based on data culled from the literature and from satellite images. These changes were analyzed alongside fluvial sediment loads. Delta shoreline mobility to changing fluvial loads has been variable, reflecting the miscellaneous factors that influence the supply of sediment to deltas. 29 deltas are in overall erosion, 18 show shoreline advance, whereas seven do not show any significant change. The sediment loads received by 42 deltas diminished relative to values prior to 1970, by more than 50% for 28 of them. Ten deltas showed advance, some significantly, notwithstanding fluvial sediment load decreases exceeding 25%. Overall, with the exception of the Colorado (Tx) and the Indus, losses in subaerial coastal area have been rather low. It would appear that diminishing fluvial sediment supply, the driving force in deltaic equilibrium at a multi-decadal timescale, has not, thus far, had a significant negative impact on multi-decadal delta shoreline mobility. This is important in terms of gauging currently perceived delta vulnerability. Notwithstanding, a clear link exists between the mobility of delta shorelines and the reduction in fluvial sediment loads. Eroding deltas have been affected by a reduction that is twice as important as that of stable or advancing deltas since 1970. Dams currently in place will reduce, in the future, the sediment load to their deltas of 25 of the 54 rivers by more than 50% and 100% for 15 of them. It is important to envisage the supply of sediment to deltas less in terms of its direct role in generating accretion, and eventual delta shoreline advance, and more in terms of an agent of resilience. The reduction of fluvial sediment supply to deltas will negatively impact their resilience to other drivers in the future: anthropogenic, climate change, and sea-level rise. The variability of delta shoreline behavior in the face of changing fluvial sediment loads also calls for more in-depth studies of individual deltas in order to build up future management plans addressing vulnerability and loss of resilience to marine forcing, subsidence, and sea-level rise.

*Keywords:* River deltas, Delta shoreline mobility, River sediment supply, Dams, Delta vulnerability, Delta erosion

## 1. Introduction

River deltas are a major and coveted asset for countries that have them within their borders, and their future is emerging more and more as an important societal concern. Deltas are home to hundreds of millions of people, and, commonly characterized by fertile wetlands, they form rich and bio-diversified ecosystems at the interface between land and water (Ericson et al., 2006; Overeem and Syvitski, 2009; Brondizio et al., 2016; Day et al., 2016; Seijger et al., 2016; Hagenlocher et al., 2018). Many deltas provide mineral and organic resources, and commonly host agricultural, tourist, transport networks, and port and shipping activities, while ensuring the provision of a variety of other ecosystem services such as recreation, ecological conservation, water supply, and protection, by their shorelines, against storms and marine submersion (Evans, 2012).

Deltas depend, however, on sustained sediment supply, principally from the river basins they are part of, to keep up with forcing and maintain aggradation, and eventually, to prograde. Aggradation defines vertical sediment accumulation, and progradation the seaward advance of a shoreline under conditions of adequate sediment supply (Anthony, 2016). Healthy deltas are, thus, characterized by adequate sediment supply to balance marine forcing, subsidence (sinking) under the weight of new sediment deposited on the surface of the delta, or generated by human activities, and sea-level rise. Eventually, under these conditions, surplus sediment contributes to delta shoreline advance seaward. The advantages provided by deltas also imply feedback wherein their geological development and their ecosystems have been commonly influenced by societal, cultural and economic factors. The inception, growth, and decline of numerous large and small deltas in the world have been strongly influenced by human population dynamics and interventions on catchments over the last six thousand years, notably land-use changes resulting in changing fluvial sediment loads (e.g., Ruddiman, 2003; Anthony et al., 2014). Whereas past pressures have been important in the Mediterranean and in Asia in the wake of the rise and fall of societies, many deltas in these two areas, but also in other areas of the world, are currently subject to continuously growing pressures in the face of economic development and population growth. The theme of human influence on how deltas currently evolve, and are likely to do so in the future, has, thus, become an overarching one in modern delta studies, especially in the present times of climate change and sea-level rise (Ericson et al., 2006; Syvitski and Saito, 2007; Syvitski, 2008; Syvitski et al., 2009; Foufoula-Georgiou, 2013; Ibáñez et al., 2014; Tessler et al., 2015, 2018; Brondizio et al., 2016; Dunn et al., submitted).

Over the last few decades, human impacts, coupled with the effects of climate change, are rendering many deltas economically and environmentally vulnerable. Deltaic systems can be anthropogenically affected in a variety of ways but the main sources of perturbation are increasing urbanization, the construction of dams dedicated to irrigation and hydropower production, land-use changes and mining activities in catchments, the extraction of channel-bed sediments to ensure fluvial navigation and provide aggregate for construction purposes, the regulation of river flow by channeling, and the building of embankments and dikes (Evans, 2012; Kondolf et al., 2014; Day et al., 2016; Besset et al., 2017; Best, 2018; Hagenlocher et al., 2018). Reduced sediment supply to deltas potentially generates a reduction in subaerial delta area, but also renders deltas more vulnerable to erosion, given the ancillary role of sediments accumulating in deltas in dissipating fluvial, wave, and current energy (Anthony, 2014). This reduction in area can have dramatic consequences on delta populations. Sediment reduction impairs the ability of deltas to balance subsidence, and can lead to shrinking of the delta through landward shoreline mobility. Such changes can result in the deterioration and eventual disappearance of various ecosystem services provided by deltas.

Whereas the effects of accelerated subsidence and sea-level rise on river deltas have received attention in recent years, notably synthesized by Ericson et al. (2006) and Syvitski et al. (2009), and more recently by Tessler et al. (2018), delta shoreline mobility has been treated in numerous case studies rather than in a synthetic approach. Notwithstanding, there is a lack of crucial reliable data on subsidence rates for deltas, although this situation may change with increasing recourse to remote sensing data (Higgins, 2016), combined with inundation modelling (Gebremichael et al., 2018). The difficulties of actually correctly measuring changes in delta surface elevation over large tracts of a delta plain in fact mean that shoreline changes, much more easily identified through increasingly available and higher-resolution satellite images (Donchyts et al., 2016; Pekel et al., 2016), could be a useful indicator of delta stability and vulnerability. In this paper, we further expand on the theme of the relationship between river sediment supply and recent multi-decadal delta shoreline change by reviewing the current status of 54 of the world's deltas (Fig. 1), based on the assumption that the net long-term mobility of a delta's shoreline crucially depends on sediment supply from its river catchment. We bear in mind that shoreline mobility can be influenced by various other factors such as subsidence, sea-level change, and apportionment of sediment in the coastal zone among channels, shorelines, and the delta plain. Deltas are also influenced by marine forcing and, notably, by high-energy events such as storms and tsunami, but we also assume that delta shorelines evince resilience to such short-term events. In addition to fluvial sediment supply, some deltas can also be sourced by shoreface sediments, especially in wave-dominated settings where abandoned lobes

are reworked to supply sediment to the shore. Finally, delta shoreline mobility can be influenced by shoreline engineering. We assume, however that, with the exception of sea-level rise, these other sources of shoreline mobility or stabilization play a much less determinant role, at multi-decadal and longer timescales, than fluvial sediment supply.

## 2. Data and methods

### 2.1. Choice of deltas

We analyzed 54 of the world's deltas (Fig. 1) with a choice based mainly on a compromise struck between the twin criteria of availability of data from databases and scientific publications and delta size. The largest deltas are commonly those subject to the most important anthropogenic pressures, although there are noteworthy examples of large deltas still relatively preserved from such pressures. A number of small deltas (see section *3.1.3*) were also included in order to evaluate whether delta size was a criterion in delta vulnerability related to diminishing fluvial sediment supply. A third additional criterion consisted in adjusting the list of selected deltas in order to offer as much a balanced world view as possible (Fig. 1). We did not take into account the subaqueous parts of the selected deltas. Subaqueous delta area is rather poorly documented in many of the sites retained in this review. Nevertheless, there are quite a number of large deltas, notably muddy deltas, the subaqueous parts of which are much more voluminous than the subaerial parts, as in the cases of the Ayeyarwady and the Amazon. The review is based on the confrontation of delta shoreline changes with changes in river sediment supply.

### 2.2. Shoreline change

Data on shoreline change for the 54 deltas were derived from two metrics: (1) shoreline mobility and induced coastal area change over time, and (2) conversion of coastal land into water, or conversion of adjacent coastal water into land.

#### 2.2.1. Shoreline mobility and area change

Quantification of the historical evolution of the delta shorelines was based on a prior compilation for each delta culled from the literature (Table 1). Some of these studies were devoted to a delta in particular, while others covered several deltas. The closure years for the analysis are 2013, 2014, or 2015. Where necessary, we completed the coverage up to 2015 (Table 1).

Complementary analysis of shoreline mobility and area change was carried out from a heterogeneous spatial database consisting of orthorectified satellite images of medium to high resolution:

mostly Landsat[®] (U.S. Geological Survey (USGS), 79 - 30 m pixel size), SPOT[®] 5 (European Space Agency (ESA) /ISIS, 2.5 m pixel size), and SPOT[®] 6 (ESA/GEOSUD, 1.5 m pixel size), depending on availability over the period 1972 – 2015 (see Supplementary Material 1). For deltas impacted by seasonal monsoon and monsoon-type changes, all analyzed images covered the dry season. Images were also selected following a scrutiny of hourly tidal data to ensure homogeneity of the water level on all the images of the same site, favouring, wherever possible, high-tide images that are the most appropriate for delimiting the shoreline. End-of-year images were lumped with those of the following year. The spatial dataset was selected to cover the entire delta coastline for each year analyzed, with a minimum cloud cover of less than 10% (sorted in the USGS database for Landsat[®] imagery).

### 2.2.1.1. Shoreline delimitation

In view of the heterogeneous resolutions of the spatial data, the delta shoreline was delimited by operator photo-interpretation. Although this manual method may appear long and tedious, we preferred it to automatic methods (e.g., Shaw et al., 2008) because it offers the possibility of involving a much less number of steps than the latter, while good operator judgement can reduce bias in the recognition of the deltaic land-sea interface, a potentially complicated and dynamic zone that can be associated with large fluctuations in tidal range, large volumes of suspended sediments, more or less discernible dunes toes, and seasonal freezing. Manual operator delimitation also has the advantage of enabling identification and referencing of various other shoreline aspects on these deltas (vegetation, land-use) that are not the object of the present study. Since the objective here is to statistically analyze the multi-decadal shoreline evolution trends, we excluded potential shoreline markers subject to instantaneous, daily, or event-related fluctuations, such as swash zones or dune toes. The seaward boundary of mature vegetation cover is considered as a clean and usable limit for mangrove- and other types of forest-bound shorelines (Coyne et al., 1999; Guy, 1999; Priest, 1999; Trépanier et al., 2002). A mature vegetation cover is a reliable indicator of the shoreline, regardless of the resolution of satellite images. In order to distinguish areas of mature, and especially long-established, vegetation from sparse, growing or eroding vegetation, we used a combination of three spectral bands of Landsat satellite imagery. Bands 4 and 5 in the near infrared and band 7 in the mid-infrared provide a clear composition because the concerned wavelengths are attenuated by water, in particular in the shoreline area. With this combination, the vegetation is bright blue on the satellite image when healthy and dense, but dull blue when sparse or stressed. On engineered deltaic shorelines, we selected the seaward limit of protective structures such as dikes and embankments, as well as roads and canals in cultivated areas (Morton and Speed, 1998; Coyne et al., 1999; Guy, 1999). The shorelines on

Landsat[®] images were digitized with a magnification ranging from 1:8000 to 1:20,000, whereas this ranged from 1:5000 to 1:8000 for SPOT[®] images. Vector points were set over distances of 30 to 100 m depending on the resolution of the image. A plot was made directly on the computer screen with a 0.35 mm thick cursor in ArcGIS[©] GIS. Shoreline detection is the most delicate step as it combines uncertainties (see below) related to image georeferencing, resolution, the thickness of the cursor, and the appreciation and experience of the operator, in addition to image quality aspects related notably to cloudiness. Figure 2 shows examples of successive delimited shorelines for the Ebro delta.

### 2.2.1.2. Surface area change and uncertainties

Using GIS, we determined surface area differentials between shorelines of different dates (about a year interval depending on available data) in terms of annual area gains and losses. The calculated total error $E_p$ [m] generated by shoreline digitizing corresponds to the sum of the error relative to image resolution $E_r$ [m], the root mean squared georeferencing errors $E_g$ [m] of the data, and the precision of the cursor $E_c$ [m] used to vectorize the shoreline, expressed by:

$$E_p = \sqrt{E_r^2 + E_g^2 + E_c^2} \tag{1}$$

We georeferenced the satellite images by using a first-order polynomial transformation. The measured error (residue error) is the difference between the final position of the origin point relative to the specified real location (destination point). $E_p$ is the sum of the mean squared errors of all the residues. The individual errors are expressed as a ratio relative to the spatial scale used (Fletcher et al., 2003; Rooney et al., 2003; Hapke et al., 2006). $E_c$ averaged is 2.8 m, based on the thickness (0.35 mm) of the cursor used to vectorize the shoreline and the mean scale (1:8000) used to visualize the satellite images on the GIS interface. Some parameters taken into account in the uncertainty determined by these authors are not documented for the spatial data used, such as the error related to tidal fluctuations (nevertheless avoided as best as possible during the selection of the satellite images).

The uncertainty $E_{AC}$ involved in the annual rate of area change (AC) of the coastal fringe (see below for definition of the coastal fringe) of each delta in [km²/year] was calculated using the following formula (Himmelstoss, 2009; Hapke et al., 2006):

$$E_{AC} = \frac{\sqrt{ShaE_{t_0}^2 + ShaE_{t_1}^2}}{t_1 - t_0} \tag{2}$$

where $ShaE_{t_0}$ and $ShaE_{t_1}$ in [km$^2$] are the averaged estimates of the area uncertainty for successive sets of images and $t_0$ and $t_1$ are the two dates studied in decimal years, respectively, the older and the more recent. $ShaE_{t_0}$ and $ShaE_{t_1}$ were obtained from the calculation of the mean squared errors of each 1-km long segment (the shoreline was partitioned into linear 1-km segments using the DSAS v4.4 tool (Thieler et al., 2017)) (Table 2). The surface area error obtained for each linear km, for each pair of dates studied, is averaged for each delta. Values ranged from 0.0072 to 0.0099 km$^2$/year. (Table 2).

The 54 river deltas vary considerably in subaerial size, and it is evident, therefore, that a same shoreline change rate does not have the same significance for two deltas with different dimensions and subjected to varied periods of analysis. In order to compare change rates, we expressed the annual coastal area change of each delta as a percentage of a standard pre-defined coastal band. We used a backshore baseline of 2 km relative to the 2015 shoreline of each delta and calculated the area within this bandwidth of 'active' coastal change (Fig. 2), referred to hereafter as the ACB. We preferred this metric, which incorporates multi-decadal changes pertinent to the shorelines rimming subaerial deltas, to both subaerial delta area, given the disparity in size among deltas and the large uncertainty in calculating the area of the subaerial delta, and a subaerial delta protrusion area (DPA) metric (Besset et al., 2017). None of the deltas analyzed showed a 30-year shoreline mobility exceeding this 2 km-wide band. The DPA, defined as the area between the current delta shoreline and a straight line behind this shoreline running across the delta plain and linking it to the adjacent non-deltaic shorelines was used to characterize multi-decadal shoreline change in 10 Mediterranean and Black Sea deltas (Besset et al., 2017). While being convenient for simple or single delta-lobe configurations typical of wave-dominated deltas, its delimitation can be too subjective when applied to deltas with one or more active or inactive interlinked delta distributary mouths, notably bayhead deltas (Simms et al., 2018). We acknowledge that calculating the area of the active coastal band might involve a degree of bias in zones of intricate curvilinear shorelines (Fig. 2), but this metric appears more appropriate for comparison than subaerial delta area and the DPA. The ACB area of the 54 deltas is shown in Supplementary Material 2.

The relative error $E_{AC_{ACB}}$ of percentage of area change of the ACB is calculated from the product of the total length of the shoreline $L_S$ in [m], and the calculated area error margin for each alongshore kilometre $E_{AC}$ in [km$^2$/yr], and then expressed as a ratio relative to the ACB in [km$^2$] over a time span T in [yr] (here 30 years) (Table 3):

$$E_{AC_{ACB}} = \frac{L_S \cdot E_{AC} \cdot 100}{ACB} T \qquad\qquad (3)$$

Change is considered insignificant when the percentage of ACB area gain or loss is below the resulting threshold value of uncertainties thus calculated.

### 2.2.2. Land/water conversion at the shoreline

Shoreline area changes determined using the method and procedures described in the foregoing sections were complemented with data downloaded from Donchyts et al. (2016) and Pekel et al. (2016) for identifying shoreline areas converted from land into water and vice versa (Fig. 3). This database consists of Landsat® satellite images covering 32 years (1984-2015). The data are derived for each pixel (30 x 30 m) of satellite image over a coastal width of 2 km relative to the 1984 shoreline, for consistency with the shoreline change bandwidth (ACB) of 2 km. The rationale for retaining this width as a common reference is that it corresponds to the bandwidth of change liable to be caused by erosion (delta land conversion into coastal water) or accretion (coastal water conversion into delta land). As in the case of the ACB, we acknowledge, however, a number of limitations with this width, such as size and roughness of the shoreline, and inclusion of water areas (lagoons) behind narrow shoreline barriers that could have silted up or been reclaimed, or land areas that have been transformed into wetlands. We will highlight examples of these limitations where appropriate. The data also show seasonal patterns of surface conversion between 1984 and 2015 for each pixel. Overall, we retained four conversion categories over the 32-year period of observation (Fig. 3): (1) new permanent water surfaces (land into permanent water, $[A_2]$), (2) loss of permanent water (permanent water into land, $[A_3]$), (3) permanent water into seasonal water $[A_4]$, and (4) seasonal water into permanent water $[A_1]$. A single category suffices to validate the presence of water. The category representing the year a change is identified is then considered as the first year of change. The category of the last year is always attributed to the last year of observation (October 2014 to October 2015).

### 2.3. Changes in river sediment load

The fluvial sediment load corresponding to the drainage basin associated with each delta was obtained from the literature or calculated for two periods: (a) prior to 1970, and (b) between 1970 and 2014. The rationale for this choice of periods is to compare sediment loads over two distinct periods in order to highlight potential variations that may be gauged against shoreline mobility over the last 30 years, and, thus, test the extent to which river delta shorelines can be used as an indicator of delta vulnerability

induced by diminishing fluvial sediment supply. Although water discharge data, on which are based calculations of sediment loads (see below), may date back several decades for some rivers, many others do not have data going far back before 1970. This year is close to the 1968 peak in world-wide commissioning of dams that commonly necessitated the acquisition of hydrological data a few years prior to dam projects (Beaumont, 1978; IPCC, 2014; Cook, 2017). The pre-1970 sediment loads were collated from the literature for the Adra, Arno, Brazos, Ceyhan-Seyhan, Colorado (Mx), Danube, Ebro, Fly, Grijalva, Guadalfeo, Indus, Krishna, Mackenzie, Magdalena, Magra, Mahanadi, Mangoky, Medjerda, Mississippi, Moulouya, Nile, Ombrone, Orange, Parana, Pearl, Po, Rhône, Sao Francisco, Shatt el Arab, Tana, Vistula, Volta, Yellow, Congo, and Zambezi (Table 4), whereas those of the other 18 rivers were estimated from calculations based on the annual water discharge available for the years up to 1970. The post-1970 sediment loads were obtained from the literature for 52 deltas (Table 4), whereas those of the Colville and Mangoky were estimated from calculations based on the annual water discharge, using the same method as for the pre-1970 sediment load calculations. Water discharge data were obtained from the Global Runoff Data Centre (https://www.bafg.de/GRDC/EN/Home/homepage_node.html, see Supplementary Material 3).

To estimate the pre- and post-1970 sediment loads, $Q_s$ [kg/s], from the mean annual water discharge $Q$ [m$^3$/s], we used the formula of Syvitski and Morehead (1999):

$$Q_S = 25.19\, Q^{-2.209} \cdot Q^{\left(\left[\frac{\left[\log\left(\frac{0.02 H^{1.5} A^{0.5}}{25.19\, Q^{-2.209}}\right)\right]}{\log Q}\right]-1-0.238\right)+1} \tag{4}$$

where $H$ is the maximum elevation of the catchment area [m] and $A$ the area of the catchment [m$^2$].

This equation can be expressed in the simplified form:

$$Q_S = aQ^{b+1} \tag{5}$$

where:

$$a = 25.19\, Q^{-2.209} \tag{6}$$

$$b = \left[\log\left(\frac{0.02 H^{1.5} A^{0.5}}{a}\right)\right] - 1 - c \tag{7}$$

The rationale for this choice is that once flows of less than 20 m$^3$/s are excluded, the sediment concentration rate [kg/m$^3$] can be estimated from $Q$, representing 65% of the variance in the course of

experiments carried out on a sample of 36 rivers (Syvitski et al., 1998a, b), with $c = 0.238$, where $c$ is the organic regression coefficient used to convert the daily sediment load into an average annual sediment load. Using historical data on water discharge (see hydrometric stations in Supplementary Material 3), we calculated the sediment load for each year of analysis.

Estimation of the sediment load of a number of rivers can be affected by sediment trapping behind dam reservoirs. The sediment loads trapped by dams were calculated from the sediment concentrations of the main channels, $C_S$ [kg/m$^3$] obtained for each river from the sediment load $Q_S$ [kg/s] and the average annual flow rate $Q$ [m$^3$/s]:

$$C_S = \frac{Q_S}{Q} \tag{8}$$

By simply converting the mass and time units, the sediment load is expressed in tons per year. The sediment concentration is also used to determine the theoretical mass of sediment that can be stored in one year ($C_{S_{stored}}$) in the volume of existing reservoirs ($V_{storage}$):

$$C_{S_{stored}} = C_S \cdot V_{storage} \tag{9}$$

Once converted into tons, this mass is subtracted from the annual mass of sediments delivered by the river. Thus, the percentage of sediments retained by the reservoirs in one year, in the case of storage reaching maximum capacity, can be estimated.

Only orders of magnitude and the tendency for loads to increase or decrease are exploitable, because of the lack of hydrometric stations covering the entire drainage basins. Although the flow of each tributary joining the mainstem channel is taken into account, only the potentially transportable solid load to the coast can be calculated from the flow volumes, and assuming that no obstacle, such as water retention by a reservoir dam, alters these volumes downstream. For 16 rivers, this is indeed the case (Fig. 4). Up to 20 dams and reservoirs, constructed after 1970, are located downstream of the flow measurement stations of these rivers. The cumulative storage capacities of these are of the order of ten million m$^3$ to a hundred km$^3$, as in the case of the Orinoco river. Although we know that these dams exist downstream, it is not possible to adjust the flow volumes obtained upstream because there are no reliable and continuous data on what is actually retained by these dams. However, these volumes give an idea of the underestimation of the sediment load reduction for 13 rivers having a negative sediment balance: Brazos, Chao Phraya, Colorado (Tx), Godavari, Indus, Medjerda, Murray, Rhône, Senegal, Shatt el Arab,

Mississippi, Volta and Chang Jiang. On the other hand, for the Dnieper, Orinoco and Parana, the increases in sediment load are overestimated, especially as the retention capacities of the dams downstream of the stations on their mainstems are among the most important.

The fact that the data extracted from the literature or calculated from time series of available water discharges (Table 4) are not homogeneous in terms of dates, but only ascribed to a period (pre- or post-1970) constitutes a limitation that should be kept in mind. However, comparison of the pre- and post-1970 values yields the same important information on the order of magnitude and the trend of evolution of fluvial sediment supply.

## 3. Results

### 3.1. Delta shoreline mobility

#### 3.1.1. Global situation

The evolution of the 54 deltas has been variable. Seven deltas (13%), the Murray, Po, Cunene, Adra, Arno, Shatt el Arab and Magra, showed percentages of area change within their respective ACB error margins, corresponding to no significant change. The remaining 47 deltas showing significant change are depicted in Fig. 5, of which 29 (53.7%) exhibited retreat and loss of coastal area with a maximum rate of -8.55 km$^2$/yr for the Mississippi (Fig. 5a, b). ACB area losses for the most severely affected deltas attained 20.5% for the Colorado (Tx) and 15.2% for the Indus. The Ombrone (-0.18%), Rhône (-0.47%), Guadalfeo (-0.66%), Sao Francisco (-0.68%) and Dnieper (-0.68%) showed the lowest ACB area losses.

Only 18 deltas (33.3%) gained ACB area over the study period (Fig. 5a, b). Among these, the Chang Jiang showed a maximum, with a 49% overall increase, corresponding to +18.5 km$^2$/year. The Pearl (35%), Red River (23%), and Parana (12%) also registered significant gains. These five deltas are among the largest. The smallest gains were those of the Danube (0.11%), Tana (0.17%) and Congo (0.35%). The larger the ACB, the larger the change rate tendency in both advancing and eroding deltas (Fig. 6).

#### 3.1.2. Spatial and temporal variations in delta shoreline change

All deltas showed more or less marked spatial and temporal variability in shoreline mobility. This is to be expected given the complexity of delta behavior in space and time, especially where more than one delta lobe is present. Figure 7 depicts coastal area gains and losses for a selection of some of the large

deltas. The total area gained by the Ganges-Brahmaputra (GB) delta, i.e. +33.87 km$^2$/year, in the present area of the active distributary mouths, was nearly balanced by an overall area loss of 26.47 km$^2$/year in the abandoned lobes of the Sundarbans. The overall rate of evolution of the GB was, thus, much higher than that of the other deltas but, compared to its ACB area, this change rate was relatively low. A similar behavior is observed for the Mekong, Ayeyarwady, Mississippi and Indus deltas which have lost and gained, annually, several km$^2$ depending on the sectors.

The mobility pattern over time has also been quite variable (Fig. 8). Non-parametric Mann-Kendall tests further highlight this variability with some deltas showing a temporal trend and others not. The Orange, Orinoco, Chang Jiang and Vistula all show an increasing trend in area gain, whereas the Mekong and Paraiba do Sul show a downward trend. Among dominantly eroding deltas, the Mississippi, Volta, Moulouya, Arno, Magdalena, Limpopo, Rhône, and Mackenzie show a trend of decreasing erosion. The Indus, Medjerda, Godavari, Krishna, Ebro, and Shatt el Arab, show, on the other hand, an aggravation over time of their erosion.

### 3.1.3. Dichotomy between small and large eroding deltas

We distinguished small from large deltas by setting a limit between the two categories using the first quartile in ACB area ranking. This limit corresponds to 400 km$^2$ (Fig. 9), with 27 (50%) in the small category. In both categories, shoreline retreat has dominated. Among the 27 large deltas, 11 (40.7%) underwent retreat, whereas 19 of the 27 small deltas (70.4%) suffered the same fate. Losses for the large delta category averaged 8.7%, whereas small deltas lost, on average, 3.7% of their ACB. However, among the 27 large deltas, only 11 (40.7%) underwent retreat, whereas 19 of the 27 small deltas (70.4%) suffered the same fate. Another notable difference between the two categories is the moderately high (18.5%) percentage of small deltas with stable shorelines, compared to large deltas (7.4%).

### 3.1.4. Land/water conversion of the ACB

Thirty-four (63%) of the 54 deltas were dominated by conversion of land into permanent or seasonal water. 39 (72%) exhibited a larger transformation of coastal land to permanent water than of coastal water into land (Fig. 10). A comparison of these transformations with the 18 deltas showing a gain in ACB area shows that 6 deltas (33%) were dominated by transition towards more conversion of land into permanent water than of conversion of water into permanent land. Among the 29 deltas that have undergone a loss of ACB area, 21 (72%) were dominated by conversion of land into permanent or seasonal water, and 18 (62%) exhibited more conversion of coastal land into permanent water than of

coastal water into permanent land. Among the seven deltas showing no significant change in ACB area over the period of analysis, six (86%) were dominated by conversion of more land into permanent water than of conversion of more water into permanent land.

### 3.1.5. Sediment loads

The changes in sediment load are depicted in Fig. 11 together with the percentage of load change between the pre- and post-1970 periods. For 38 rivers, the load has diminished by more than 20%. The decrease has been particularly important in Mediterranean deltas: Nile, Ebro, Magra, Moulouya, Ombrone, and Rhône, exceeding 80%, but also in ten other deltas: Colorado (Mx), Grijalva, Orange, Krishna, Yellow River, Red River, Pearl, Mississippi, Volta and Chao Phraya. Several other deltas are, however, associated with catchments that have registered mild increases in sediment loads: Zambezi, Amazon, Dnieper, Ganges-Brahmaputra, Parana, Colville, Mackenzie, Magdalena, Limpopo, Mangoky, Vistula, and Fly (Fig. 11).

## 4. Discussion

This review shows that 29 out of 54 deltas, of which 11 in the large (ACB area > 400 km$^2$) category, have been undergoing erosion over the last three decades (Figs. 5, 8, 9). This trend is consistent with a larger conversion of land into water, within the 2 km-wide ACB, than of water into land (Fig. 10). At the same time, the fluvial sediment loads associated with 42 deltas have diminished significantly (Fig. 11). The clear dominance of coastal erosion indicates that the shorelines rimming these deltas no longer dispose of the supply of sediment necessary to balance forcing and induced alongshore/offshore sediment redistribution beyond the confines of the subaerial delta. This having been said, however, with the exception of the cases of the Colorado (Tx) and the Indus, losses in delta ACB have been rather low. In the large delta category, the average loss in ACB area diminishes from 8.7% to 2.8% when the Indus (-15.2%) is excluded. This is an important finding in terms of gauging currently perceived delta vulnerability, and would tend to indicate that, over the last three decades, diminishing fluvial sediment supply, the driving force in deltaic equilibrium at a multi-decadal timescale deltas, has not, thus far, had a significant negative impact on delta shoreline mobility. Notwithstanding fluvial sediment load decreases exceeding 20%, ten deltas in fact showed gains in ACB area, some very significantly. Given the diversity of the context of deltas, the strength and quality of the relationship between shoreline mobility and coastal area losses or gains are affected by a whole range of miscellaneous factors that include: (1) direct

sediment retention by dams and reservoirs, and, increasingly, channel-bed mining and river engineering; (2) given the commonality of bedload in constituting delta shorelines, variable lag in the downstream propagation of the effect of bedload trapping by reservoirs, and attendant bedload transfer, downstream of dams, from river channels to delta shorelines, as well as potential upstream-to-downstream changes in the distribution of sediment source-and-sink areas; (3) the effects of mining and land-use changes that strip catchments of vegetation, resulting in enhanced sediment supply, or the counter-active impact of reforestation that protects catchment slopes from erosion; (4) differences in sensitivity to sediment reduction between the subaerial and the subaqueous parts of a delta, and deltaic self-organization involving, for instance, sediment apportionment among channels, shorelines, the subaqueous delta, and the subaerial delta, in addition to processes such as channel switching and lobe abandonment; (5) delta shoreline advance due to land reclamation, or the mitigating effects of engineering structures in protecting eroding delta shorelines, or in trapping sediment that would, otherwise, be reworked and evacuated alongshore or offshore; (6) aggravated subsidence due to human activities; and (7) the impact of enhanced storminess and episodic high-energy events where delta resilience is already impaired by dwindling sediment supplies. Land reclamation, for instance, has been particularly important in the two deltas that show the most important gains in ACB, despite a diminishing sediment supply: the Chang Jiang, where 840 km$^2$ of wetlands were converted to land between 1950 and 1995 (Fan et al., 2006), and the Pearl delta with a reclaimed area of 356 km$^2$ between 1988 and 1997 (Deng and Bao, 2011; Wu et al., 2016). In both deltas, the 2 km-wide shoreline band for land-water conversion and for defining coastal area change used as a reference in our study was extended seaward (Fig. 10). In other deltas, such as the Rhône, lagoon infill has also occurred locally over the last few decades, expanding the water-to-land conversion in the 2 km-wide coastal band, thus mitigating loss in ACB area.

Our review shows that small deltas (ACB area ≤ 400 km$^2$) tend, proportionately to their number in this study (27/54), to be more prone to erosion compared to the larger (ACB area > 400 km$^2$) deltas (Fig. 9). It is likely that the smaller deltas are more sensitive to the effects of sediment sequestration by dams and reservoirs on their watersheds, whereas these effects are more likely to be more readily dampened or slowed down in catchments with large deltas. These small deltas also generally have small river sediment inputs (Table 4, Fig. 12) which may explain a greater sensitivity to marine reworking and erosion, especially by waves (Anthony, 2015; Nienhuis et al., 2015). The results suggest, thus, that small deltas, which have tended to attract less attention than large deltas, could, in fact, be relatively more vulnerable and less resilient. This is an important point to ponder as many small deltas also support dense populations and valuable activities, as in the Mediterranean (Anthony et al., 2014). In contrast, small deltas have a

comparatively much higher percentage of stable shorelines (Fig. 9), and this may reflect the potentially relatively lower costs involved in engineered stabilization of the short shorelines rimming these smaller deltas, such as the Magra and the Arno (Anfuso et al., 2011), and the Adra (Jabaloy-Sánchez et al., 2014), compared to large deltas with longer shorelines.

Although delta shoreline mobility does not appear, thus far, to have been strongly negatively impacted by diminished fluvial sediment loads, there is, nevertheless a clear relationship between these two parameters (Fig. 12). The linear relation yielded by the regression is poor when all deltas are taken into account. However, exclusion of eight outliers yields a statistically significant relationship that confirms the importance of fluvial sediment supply in determining ACB (and subaerial delta) area. Among the eight outliers, four are North American deltas: Mississippi, Mackenzie, Colville, Grijalva. These deltas, notably the Mississippi and the Mackenzie, have a relatively large ACB area relative to their current sediment supply, thus reflecting not only the effects of prolonged sediment reduction due to dams (the case notably of the Mississippi), but also the relatively sheltered Gulf Coast and Arctic settings of these deltas. Three of these deltas (Mississippi, Mackenzie, Colville) show intricate shorelines that generate a high ACB area (Figs. 5, 12). The other four outliers are African deltas (Orange, Cunene, Moulouya, Medjerda) that show a small ACB area relative to their sediment supply, thus possibly indicating either a high-energy wave-dominated context (Cunene, Orange) or prolonged past erosion due to sediment trapping by dams, as in the cases of the Moulouya and Medjerda (Besset et al., 2017).

The synthesis in Fig. 13 highlights the importance of fluvial sediment supply to delta shoreline mobility. Eroding deltas are associated with a reduction in fluvial sediment supply that is twice as important as that of stable or advancing deltas. When grouped together, eroding deltas receive less than a quarter of the fluvial sediment supply of deltas with stable and advancing shorelines. Figure 14 shows a vulnerability classification perspective based on four levels of reduction of fluvial sediment supply. While the yardstick of shoreline change is also used here as an indicator of vulnerability, this metric represents only one of various indicators of delta biophysical sustainability, and, given the variable temporal trends in delta shoreline mobility (Fig. 8), cannot be used to project rates of shoreline mobility over the coming decades. The reduction of a river's sediment flux should, however, also clearly diminish a delta's resilience to other drivers. It is important to envisage the supply of sediment less in terms of its direct role in generating accretion, and, therefore, eventual subaerial delta advance seaward, and more in terms of an agent enabling deltas to keep pace with forcing and subsidence, and to maintain their resilience. With few exceptions, deltas are expected to lose resilience and become more vulnerable as a result of decreasing fluvial sediment supply. The levels proposed in Fig. 14 point out disparities between multi-decadal change

in fluvial sediment supply and the expected trend in deltaic shoreline mobility, thus highlighting the need for research on the operation of other factors at play in determining the response and resilience of deltas to a decreasing sediment supply. This variability highlights, in particular, the need, in a management framework, for considering factors influencing the shoreline mobility of deltas individually.

We have synthesized our results in terms of the global distribution of deltas (Fig. 15) within the four vulnerability levels proposed in Fig. 14. The region most affected by the loss of coastal deltaic area is North America, where the seven selected deltas showed significant coastal subaerial retreat, possibly reflecting the long history of dam construction in the USA (Ho et al., 2017). Among the six deltas analyzed in South America, four showed gains in area: Amazon, Orinoco, Paraiba do Sul and Parana, possibly reflecting, in the case of the first three, equatorial-tropical rain-forested catchments and relatively low anthropogenic pressures. In the densely-developed context of Europe and the Mediterranean, only the Vistula, subject to relatively low anthropogenic pressures, significantly gained in ACB in 30 years. From the Persian Gulf to the Gulf of Thailand, eight out of the nine deltas analyzed were eroding, reflecting the impact of anthropogenic pressures, while two large deltas, the Ayeyarwady and the Ganges-Brahmaputra showed gains. In the case of the former, increasing agricultural transformation of the catchment and mining have probably balanced sediment reduction loads due to dams (SOBA, 2017). Among the 10 deltas in sub-Saharan Africa, the Orange, the Congo and the Zambezi have gained coastal area, while six others were eroding and the remaining one (Cunene) did not show any significant evolution over the study period. Among the seven deltas of Pacific Asia and Oceania, five registered significant shoreline advance: Yellow River, Chang Jiang, Pearl, Red River, and Murray, whereas others showed shoreline retreat. The reasons for this variability are diverse, and include not only the effects of dams, but also those of human pressures and climate change in the river basins, and within individual deltas. This variability also underpins the importance of further analysis of individual deltas in order to implement better future management scenarios.

The erosion of deltaic shorelines in the present context of diminishing sediment supply should be a cause for concern in the coming years, given the compounding of impacts expected from climate change and sea-level rise. Mechanisms depriving deltas of sediment, or contributing to high subsidence rates, enhance the effects of sea-level rise in driving delta vulnerability (Ericson et al., 2007; Syvtiski et al., 2009; Tessler et al., 2015, 2018; Dunn et al., submitted), and this should include delta shoreline retreat. Model scenarios by Tessler et al. (2018) of the impact of contemporary and future water resource management schemes and hydropower dams in river basins on relative sea-level rise across 46 global

deltas suggest that contemporary sediment fluxes, anthropogenic drivers of land subsidence, and climate-induced sea-level rise will result in delta relative sea-level rise rates that average 6.8 mm/year. Assessment of the impacts of dams planned and under construction suggests sea-level increases of the order of 1 mm/y in deltas, whereas reduced sediment retention caused by increased river channelization and management will lead to a relative sea-level rise of nearly 2 mm/year (Tessler et al., 2018). Dunn et al. (submitted) analyzed projected changes in fluvial sediment flux over the 21st century to 47 of the world's major deltas under 12 environmental change scenarios constructed using four climate-change pathways, three socioeconomic pathways, and one reservoir construction timeline, and showed that a majority (33) of the investigated deltas are projected to experience reductions in sediment flux by the end of the century, when considering the average of the scenarios. Projected mean and maximum declines of 38% and 83%, respectively, between 1990-2019 and 2070-2099, will be driven by the effects of anthropogenic activities (changing land management practices and dam construction) overwhelming the effects of future climate change. These results highlight the consequences of direct (e.g. damming) and indirect (e.g. climate change) alteration of fluvial sediment supply to deltas.

To further gauge the impact of dams in affecting fluvial sediment loads in the future, data on the maximum sediment storage capacity behind dams erected across the 54 rivers in our study were obtained from the GRanD database (see also Lehner et al., 2011) developed in the framework of the Global Water System Project© (http://www.gwsp.org/products/grand-database.html). From the calculated fluvial sediment concentrations, the proportion of sediments that can be subtracted from the solid load of each river, in the case of a total filling of reservoirs and dams, has been estimated. In this case, these solid reservoirs would reduce the sediment load of 25 of the 54 rivers studied by more than 50% and 15 of them would be totally deprived of sediments (Fig. 16). The storage capacity by dams would be up to two to five times greater than the solid load available for the Medjerda, Zambezi, Shatt el Arab, Nile and Volta rivers. This problem will gradually appear in other rivers and become exacerbated in those already affected, given the many projects and plans (GRanD Database) as well as ongoing constructions on some rivers. These include the project on the largest hydropower dam in Africa on the Congo River, many large dams on the Zambezi River, and more than 400 dams planned along the courses of the Amazon River. Nearly 200 dams are commissioned on the Ayeyarwady River, with a total storage capacity of about 21 $km^3$, and another 25 are already planned for the beginning of the 2020s, with more than 29 $km^3$ of total retention capacity (WLE, 2017). On the Mekong River, no less than 312 dams are commissioned, with a total storage capacity that could reach more than 80 $km^3$, and 22 dams planned between 2017 and 2030, and which would store more than 25 $km^3$ water and solid load (WLE, 2017). The future of the sediment loads

of the Ganges-Brahmaputra, Mahanadi, Godavari and Krishna rivers could also be dramatically linked in the coming decades with the inception in 2015 of the largest infrastructure project in the world for irrigation, the Interlinking of Rivers Project (IRP database, http://csdms.colorado.edu/wiki/Data: NRLP India) (Bagla, 2014). This project involves linking 37 major rivers of India through thirty connections, 15,000 km of channels designed to derive 170 km$^3$ of water, and nearly 3,000 dams, including 42 major ones that could be responsible for the displacement of nearly 700,000 people (CIESIN, 2017). Beyond the risk of disturbance of the hydro-sedimentary balance of the rivers concerned, the construction of such dams will result in the submergence of more than 2.7 million hectares of cultivated, occupied or preserved land (e.g. the Panna Tiger Reserve) in India, and would force the displacement of nearly 1.5 million people. This non-exhaustive list of future dam construction projects suggests that additional pressures are to be expected on the world's deltas in the coming decades. These impending pressures urgently call for sustainable management strategies for rivers and their deltas.

## 5. Conclusions

The vulnerability status of a selection of 54 of the world's deltas was quantified from changes in delta shoreline mobility and coastal area over the last 30 years alongside fluvial sediment loads. The results show a large majority (29) of deltas in overall erosion, in a context of diminished fluvial sediment loads for 42 of the 54 rivers associated with these deltas, by more than 50% for 28 of them. Small deltas (ACB area $\leq$ 400 km$^2$) are more prone to erosion, but have tended to be stabilized by engineering. Small deltas are probably more sensitive than large deltas to the reduction of fluvial sediment supply, as well as to marine reworking and erosion, especially by waves.

When grouped together, eroding deltas receive less than a quarter of the fluvial sediment supply of deltas with stable and advancing shorelines. With the exception of the Indus, losses in delta ACB area have been rather low among the world's major deltas. These rather mild losses would tend to indicate that delta subaerial area, indexed by shoreline mobility, has, thus far, not been significantly impacted by recent changes in fluvial sediment supply, the driving force in deltaic equilibrium at a multi-decadal timescale. Delta mobility response has been variable, reflecting the miscellaneous factors that influence fluvial sediment loads, such as mitigation of the effects of dams by deforestation and mining on catchments, sediment trapping by shoreline engineering structures, and long temporal lag between dam construction and sediment reworking and transport to the coast downstream of dams. A clear link exists, nevertheless, between change in the area of the active coastal band (ACB) rimming the subaerial deltas and the

reduction in fluvial sediment loads: eroding deltas have been affected by a reduction in fluvial sediment supply that is twice as important as that of stable or advancing deltas. This reduction in river sediment flux will clearly diminish delta resilience to other drivers such as subsidence and climate-induced sea-level rise. The variability of delta shoreline behavior in the face of changing fluvial sediment loads calls for more in-depth studies of individual deltas in order to build up future management plans addressing vulnerability and loss of resilience. Dams currently in place will reduce, in the future, the sediment load to their deltas of 25 of the 54 rivers by more than 50% and 100% for 15 of them. Their potential effect, as well as the anticipated effects of climate change on fluvial sediment supply, need to be further investigated at the scale of individual deltas.

## 6. Acknowledgements

References

Adams, R., Banas, P., Baumann, R.H., Blackmon, J., McIntire, W., 1978. Shoreline Erosion in Coastal Louisiana Inventory and Assessment: Final Report to Louisiana Department of Transportation and Development. 134 pp. https://www.gpo.gov/fdsys/pkg/CZIC-gb459-4-s53-1978/content-detail.html.

Adegoke, J.O., Fageta, M., James, G., Agbaje, G., Ologunorisa, T., 2010. An Assessment of Recent Changes in the Niger Delta Coastline Using Satellite Imagery. J. Sustain. Dev., 3 (4), 277–296.

Allison, M.A., 1998. Historical changes in the Ganges Brahmaputra delta front. J. Coastal Res., 14 (4), 1269–1275. ISSN 07490208, 15515036. http://www.jstor.org/stable/4298887.

Anand Rao, M., Ramamurthy, S., Shah, B., Hanumantha Rao, V., 2006. Recent Morphological Changes Along the Krishna Delta Shoreline. J. Geol. Soc. India, 67 (5), 629–635. ISSN 0974-6889. http://www.geosocindia.org/index.php/jgsi/article/view/81924.

Anfuso, G., Pranzini, E., Vitale, G., 2011. An integrated approach to coastal erosion problems in Northern Tuscany (Italy): Littoral morphological evolution and cell distribution. Geomorphology, 129, 204–214. https://doi.org/10.1016/j.geomorph.2011.01.023

Anthony, E.J., 2014. Deltas. In: Masselink, G., Gehrels, R. (Eds.), Coastal Environments and Global Change. John Wiley & Sons Ltd., 299–337. ISBN 9781119117261. https://doi.org/10.1002/9781119117261.ch13.

Anthony, E.J., 2016. Deltas. Oxford University Press, Geoscience, Oxford Bibliographies, 32 pp. https://doi.org/10.1093/OBO/9780199363445-0057.

Anthony, E.J., 2015. Wave influence in the construction, shaping and destruction of river deltas: A review. Mar. Geol., 361, 53-78. https://doi.org/10.1016/j.margeo.2014.12.004

Anthony, E.J., Marriner, N., Morhange, C., 2014. Human influence and the changing geomorphology of Mediterranean deltas and coasts over the last 6000 years: From progradation to destruction phase? Earth Sci. Rev., 139, 336 – 361. ISSN 0012-8252. https://doi.org/10.1016/j.earscirev.2014.10.003.

Anthony, E.J., Brunier, G., Besset, M., Goichot, M., Dussouillez, P., Nguyen, V.L., 2015. Linking rapid erosion of the Mekong River delta to human activities. Sci. Rep., 5, 1–12. http://dx.doi.org/10.1038/srep14745

Arjona, S., Millares, A., Baquerizo, A., 2018. Reservoir sedimentation impact downstream in a semi-arid basin with greenhouses cultivation. In E3S Web of Conferences, 40, 03006, 8 pp. https://doi.org/10.1051/e3sconf/20184003006

Bagla, P., 2014. Water. India plans the grandest of canal networks. Science, 345 (6193), 128. ISSN 1095-9203 (Electronic). https://doi.org/10.1126/science.345.6193.128.

Beaumont, P., 1978. Man's impact on river systems: A world-wide view. Area, 10 (1), 38–41. ISSN 00040894, 14754762. http://www.jstor.org/stable/20001279.

Belperio, A.P., 1979. The combined use of was load and bed material load rating curves for the calculation of total load: An example from the Burdekin River, Australia. Catena, 6, 317-329.

Bentley, S., Blum, M., Maloney, J., Pond, L., Paulsell, R., 2016. The Mississippi river source-to sink system: Perspectives on tectonic, climatic, and anthropogenic influences, Miocene to Anthropocene. Earth Sci. Rev., 153, 139 – 174. ISSN 0012-8252. https://doi.org/10.1016/j.earscirev.2015.11.001.

Bergillos, R.J., Rodriguez-Delgado, C., Lopez-Ruiz, A., Millares, A., Ortega-Sanchez, M., Losada, M.A., 2016. Recent human-induced coastal changes in the Guadalfeo river deltaic system (southern Spain). In E-proceedings of the 36th IAHR World Congress, The Hague, Netherlands, July 2015.

Besset, M., Anthony, E.J., Sabatier, F., 2017. River delta shoreline reworking and erosion in the Mediterranean and Black Seas: the potential roles of fluvial sediment starvation and other factors. Elementa: Sci. Anthropocene, 5, 1–20. ISSN 2325-1026. https://doi.org/10.1525/elementa.139.

Best, J., 2018. Anthropogenic stresses on the world's big rivers. Nature Geoscience, 12, 7-11. https://doi.org/10.1038/s41561-018-0262-x

Bi, N., Wang, H., Yang, Z., 2014. Recent changes in the erosion - accretion patterns of the active Huanghe (Yellow River) delta lobe caused by human activities. Cont. Shelf Res., 90, 70–78. ISSN 02784343. https://doi.org/10.1016/j.csr.2014.02.014.

Billi, P., Rinaldi, M., 1997. Human impact on sediment yield and channel dynamics in the Arno River basin (central Italy). In: Human impact on erosion and sedimentation, Proceedings of Symposium S6 during the 5th Scientific Assembly of the IAHS, Rabat, Morocco, 23 April to 3 May. IAHS Publ. Vol. 245, 301–311.

Bini, M., Cararosa, N., Ribolini, A., 2008. Multitemporal (1938-2004) evolution of the Pisan shoreline based on the comparison of georeferenced aerial images (in italian). Atti della Società Toscana di Scienze Naturali, Memorie Serie A, 113, 1–12.

Brondizio, E.S., Foufoula-Georgiou, E., Szabo, S., Vogt, N., Sebesvari, Z., Renaud, F.G., Newton, A., Anthony, E.J., Mansur, A.V., Matthews, Z., Hetrick, S., Costa, S.M., Tessler, Z., Tejedor, T., Longjas, A., Dearing, J., 2016. Catalyzing action towards the sustainability of deltas. Current Opinion in Environmental Sustainability 19, 182-194. https://doi-org.insu.bib.cnrs.fr/10.1016/j.cosust.2016.05.001

Cappucci, S., Lisi, I., Ciavola, P., Rossi, L., 2015. Sediment delivery at sea by the Magra River, Northern Italy. Coastal and Maritime Mediterranean Conference, Ed 3, Ferrara, Italy, 25-30. http://dx.doi.org/10.5150/cmcm.2015.006

Cetin, H., Bal, Y., Demirkol, C., 1999. Engineering and environmental effects of coastline changes in Turkey. Northeastern Mediterranean. Environmental and Engineering Geoscience, 5, 315–330. https://doi.org/10.2113/gseegeosci.V.3.315

Chakrapani, G.J., Subramanian, V., 1990. Factors controlling sediment discharge in the Mahanadi River Basin, India. J. Hydrol. 117 (1–4), 169–185.

Chaperon, P., Danloux, J., Ferry, L., 1993. Fleuves et rivières de Madagascar. In: Monographie Hydrologique, 10, ORSTOM, Paris, 874 pp.

Chen, X., Chen, S., Dong, P., Li, X., 2008. Temporal and spatial evolution of the coastal profiles along the Yellow River Delta over last three decades. GeoJ., 71 (2), 18–199. ISSN 1572-9893. https://doi.org/10.1007/s10708-008-9155-7.

Chu, Z.X., Sun, X.G., Zhai, S.K., Xu, K.H., 2006. Changing pattern of accretion/erosion of the modern Yellow River (Huanghe) subaerial delta, China: Based on remote sensing images. Mar. Geol., 227 (1), 13–30. ISSN 0025-3227. https://doi.org/10.1016/j.margeo.2005.11.013.

Chu, Z., Yang, X., Feng, X., Fan, D., Li, Y., Shen, X., Miao, A., 2013. Temporal and spatial changes in coastline movement of the Yangtze delta during 1974-2010. J. Asian Earth Sci., 66, 166–174. ISSN 1367-9120. https://doi.org/10.1016/j.jseaes.2013.01.002.

CIESIN, 2017. NASA Socioeconomic Data and Applications Center (SEDAC) Documentation for Gridded Population of the World (GPW), v4. 4 (845), 1–51. https://doi.org/10.7927/H4B56GPT.

Cipriani, L.E., Pranzini, E., Vitale, G., Wetzel, L., 2013. Adaptation to beach erosion at Maremma Regional Park (Tuscany, Italy). Geo-Eco-Marina, 19 (1), 65–75. https://doi.org/10.5281/zenodo.56844.

Cook, H.F., 2017. The protection and conservation of water resources. John Wiley and Sons, 464 pp. ISBN 1119970040, 9781119970040.

Couvillion, B.B.R., Barras, J.A., Steyer, G.D., Sleavin, W., Fischer, M., Beck, H., Trahan, N., Griffin, B., Heckman, D., 2011. Land Area Change in Coastal Louisiana from 1932 to 2010. Technical report, USGS. U.S. Geological Survey Scientific Investigations Map 3164. https://pubs.usgs.gov/sim/3164/downloads/SIM3164_Map.pdf.

Coyne, M.A., Fletcher, C.H., Richmond, B.M., 1999. Mapping Coastal Erosion Hazard Areas in Hawaii: Observations and Errors. J. Coastal Res., SI (28), 171–184. ISSN 07490208, 15515036. http://www.jstor.org/stable/25736194.

Dada, O.A., Li, G., Qiao, L., Asiwaju-Bello, Y.A., Anifowose, A.Y.B., 2018. Recent Niger Delta shoreline response to Niger River hydrology: Conflict between forces of Nature and Humans. J. Afr. Earth Sci., 139, 222–231. https://doi.org/10.1016/j.jafrearsci.2017.12.023.

Dada, O.A., Qiao, L., Ding, D., Li, G., Ma, Y., Wang, L., 2015. Evolutionary trends of the Niger Delta shoreline during the last 100 years: Responses to rainfall and river discharge. Mar. Geol., 367, 202–211. ISSN 00253227. https://doi.org/10.1016/j.margeo.2015.06.007.

Day, J.W., Agboola, J., Chen, Z., Elia, C.D., Forbes, D. L., Giosan, L., Kemp, P., Kuenzer, C., Lane, R.R., Ramachandran, R., Syvitski, J., Ya, A., 2016. Approaches to defining deltaic sustainability in the 21st century. Estuar. Coast. Shelf S., 183 (B), 275–291. https://doi.org/10.1016/j.ecss.2016.06.018.

Deng, J., Bao, Y., 2011. Morphologic evolution and hydrodynamic variation during the last 30 years in the Lingding bay, south china sea. J. Coastal Res., SI (64), ICS2011 Proceedings, 1482–1489.

Depetris, P.J., Paolini, J.E., 1991. Biogeochemical aspects of South American Rivers: The Parana and Orinoco. In: Degens, T.E., Kempe, S., Richey, J.E. (Eds.). Biogeochemistry of major world rivers, Wiley, Chichester, UK, pp. 105–125.

De Rose, R., Prosser, I., Weisse, M., 2004. Patterns of erosion and sediment transport in the Murray-Darling Basin. Sediment Transfer through the Fluvial System (Proceedings o f a symposium held in Moscow, August 2004). IAHS Publ. 288.

Dien, T.V., Thanh, T.D., Thao, N.V., 2003. Monitoring Coastal Erosion in Red River Delta, Vietnam - A Contribution from Remote Sensing Data. Asian J. Geoinformatics, Technical Letter, 3 (3), 73–78.

Donchyts, G., Baart, F., Winsemius, H., Gorelick, N., Kwadijk, J., Van De Giesen, N., 2016. Earth's surface water change over the past 30 years. Nat. clim. change, 6 (9), 810–813. ISSN 1758-678X. https://doi.org/10.1038/nclimate3111.

Dumas, C., Ludwig, W., Aubert, D., Eyrolle, F., Raimbault, P., Gueneugues, A., Sotin, C., 2015. Riverine transfer of anthropogenic and natural trace metals to the Gulf of Lions (NW Mediterranean Sea). Appl. Geochemistry, 58: 14–25. https://doi. org/10.1016/j.apgeochem.2015.02.017

Dunn, F.E., Darby, S.E., Nicholls, R.J., Cohen, S., Zarfl, C., Fekete, B. Declining fluvial sediment delivery to major deltas worldwide in response to climate and anthropogenic drivers. Submitted, Environ. Res. Lett.

Elektrik Isleri Etud Idaresi (EIE), 1993. Sediment Data and Sediment Transport Amount for Surface Waters in Turkey, 93–59, 615. Ankara, Turkey.

El-Fishawi, N., 1989. Coastal erosion in relation to sea level changes, subsidence and river discharge. Acta Mineral. Petrograph, 30, 161–171.

Elsayed, M.A.K., Mahmoud, S.M., 2007. Groins System for Shoreline Stabilization on the East Side of the Rosetta Promontory, Nile Delta Coast. J. Coastal Res., 380–387. https://doi.org/10.2112/04-0319.1.

Ericson, J.P., Vörösmarty, C.J., Dingman, S.L., Ward, L.G., Meybeck, M., 2006. Effective sea-level rise and deltas: Causes of change and human dimension implications. Glob. Planet. Chang., 50, 63–82. https://doi.org/10.1016/j.gloplacha.2005.07.004.

Evans, G., 2012. Deltas: the fertile dustbins of the world. P. Geologist. Assoc., 123, 397–418. https://doi.org/10.1016/j.pgeola.2011.11.001.

Fan, D., Guo, Y., Wang, P., Shi, J.Z., 2006. Cross-shore variations in morphodynamic processes of an open-coast mudflat in the Changjiang delta, china: With an emphasis on storm impacts. Cont. Shelf Res., 26 (4), 517 – 538. ISSN 0278-4343. https://doi.org/10.1016/j.csr.2005.12.011.

Fanos, A.M., 1995. The impact of human activities on the erosion and accretion of the Nile Delta coast. J. Coastal Res., 11 (3), 821–833. http://www.jstor.org/stable/4298355.

Fletcher, C., Richmond, B., Rooney, J., Barbee, M., Lim, S.C., 2003. Mapping Shoreline Change Using Digital Orthophotogrammetry on Maui, Hawaii. J. Coastal Res. SI, 38 (38), 106–124. ISSN 0749-0208. http://www.jstor.org/stable/25736602.

Foufoula-Georgiou, E., 2013. A vision for a coordinated effort on delta sustainability in: Young, G. & Perillo, G.M (eds.), Deltas: Landforms, Ecosystems and Human Activities. IAHS Publications 358, Gothenburg.

Frangipane, A., Paris, E., 1994. Long-term variability of sediment transport in the Ombrone River basin (Italy). Variability in Stream Erosion and Sediment Transport (Proceedings of the Canberra Symposium December 1994). IAHS Publ. no. 224, 317-324.

Frihy, O.E., Nasr, S.M., El Hattab, M.M., El Raey, M, 1994. Remote sensing of beach erosion along the Rosetta promontory, northwestern Nile delta, Egypt. Int. J. Remote Sens., 15 (8), 1649–1660. https://doi.org/10.1080/01431169408954197.

Gebremichael, E., Sultan, M., Becker, R., El Bastawesy, M., Cherif, O., Emil, M., 2018. Assessing land deformation and sea encroachment in the Nile delta: A radar interferometric and inundation modeling approach. J. Geophys. Res.- Sol. Ea., 123 (4), 3208–3224. https://doi.org/10.1002/2017JB015084.

Goudie, A., Viles, H., 2016. Fluvial Processes and Forms in the Anthropocene. In Geomorphology in the Anthropocene, 130-178. Cambridge: Cambridge University Press. doi:10.1017/CBO9781316498910.007

Graniczny, M., Janicki, T., Kowalski, Z., Koszka-Maron, D., Jeglinski, W., Uscinowicz, S., Zachowicz, J., 2004. Recent development of the Vistula River outlet. Pol. Geol. Ins Spec. Pap., 11 (January), 103–108. ISSN 15079791.

Gupta, H., Kao, S.J., Dai, M., 2012. The role of mega dams in reducing sediment fluxes: A case study of large Asian rivers. J. Hydro., 464-465, 447-458. http://dx.doi.org/10.1016/j.jhydrol.2012.07.038

Guy, D.E., 1999. Erosion Hazard Area Mapping, Lake County, Ohio. J. Coastal Res., SI (28), Coastal Erosion Mapping and Management, 185–196. ISSN 07490208, 15515036. http://www.jstor.org/stable/25736195.

Hagenlocher, M., Renaud, F.G., Haas, S., Sebesvari, Z., 2018. Vulnerability and risk of deltaic social ecological systems exposed to multiple hazards. Sci. Total Environ., 631-632, 71–80. ISSN 18791026. https://doi.org/10.1016/j.scitotenv.2018.03.013.

Hay, B. J., 1987. Particle flux in the western Black Sea in the present and over the last 5000 years: temporal variability, source, and transport mechanisms: Unpub. Ph.D. thesis, WHOI-MIT, Cambridge, MA, 201 p.

Hapke, C.J., Reid, D., Richmond, B.M., Ruggiero, P., List, J., Hapke, C.J., Reid, D., Richmond, B.M., Ruggiero, P., List, J., 2006. National Assessment of Shoreline Change Part 3: Historical Shoreline Change and Associated Coastal Land Loss Along Sandy Shorelines of the California Coast National Assessment

of Shoreline Change Part 3: Historical Shoreline Change and Associated Coast. Open-file Report, 72 pp. https://pubs.usgs.gov/of/2006/1219/.

Harris, P.T., 1991. Sedimentation at the junction of the Fly River in the northern Great Barrier Reef, in Lawrence, D., Cansvield-Smith, T. (Eds.), Sustainable Development for Traditional Inhabitants of the Torres Strait Region: Townsville, Queensland, Great Barrier Reef Marine Park Authority, 59-85.

Hedley, P.J., Bird, M.I., Robinson, R.A.J., 2010. Evolution of the Irrawaddy delta region since 1850. Geogr. J., 176 (2), 138–149. https://doi.org/10.1111/j.1475-4959.2009.00346.x.

Heimann, D.C., Sprague, L.A., Blevins, D.W., 2011. Trends in Suspended-Sediment Loads and Concentrations in the Mississippi River Basin, 1950-2008. Scientific Investigations Report 2011-5200, U.S. Geological Survey, Reston, VA, 33 pp. https://doi.org/10.3133/sir20115200

Hereher, M.E., 2011. Mapping coastal erosion at the Nile Delta western promontory using Landsat imagery. Environ. Earth Sci., 64 (4), 1117–1125. ISSN 1866-6280. https://doi.org/10.1007/s12665-011-0928-9.

Hese, S., Overduin, P., 2014. Arctic River Delta Change Analysis with Rapid Eye Data Concepts & Challenges Intro. In 6th RESA User Workshop, Resa 473, 22 pp., Bonn, March 2014.

Higgins, S.A., 2016. Review: Advances in delta-subsidence research using satellite methods. Hydrogeol. J., 24 (3), 587–600. ISSN 1435-0157. https://doi.org/10.1007/s10040-015-1330-6.

Himmelstoss, E., 2009. DSAS 4.0 Installation Instructions and User Guide. U.S. Geological Survey OpenFile Report 2008-1278, 3, 79 pp. ISSN 2331-1258. http://woodshole.er.usgs.gov/project-pages/DSAS/version4/data/DSASv4{_}3.pdf.

Holeman, J.N., 1968. The sediment yield of major rivers of the world: Water Resources Res., 4, 737-747.

Ho, M., Lall, U., Allaire, M., Devineni, N., Kwon, H. H., Pal, I., Raff, D., Wegner, D., 2017. The future role of dams in the United States of America, Water Resour. Res., 53, 982-998. 10.1002/2016WR019905.

Ibáñez, C., Day, J.W., Reyes, E., 2014. The response of deltas to sea-level rise: Natural mechanisms and management options to adapt to high-end scenarios. Ecological Engineering, 65, 122-130.

Idroser. 1994. Aggiornamento ed integrazione del Piano progettuale per la difesa della costa adriatica emiliano-romagnola. Relazione generale. Regione Emilia-Romagna, Bologna: 276 pp.

IPCC, 2014. Climate Change 2014: Synthesis Report. Contribution of Working Groups I, II and III to the Fifth Assessment Report of the Intergovernmental Panel on Climate Change. In: Core Writing Team, Pachauri RK, Meyer LA (Eds.), IPCC, Geneva, Switzerland, 151 pp., 1–112. ISSN 1476-4687. https://doi.org/10.1017/CBO9781107415324.

Jabaloy-Sánchez, A., Lobo, F.J., Azor, A., Bárcenas, P., Fernández-Salas, L.M., del Río, V.D., Pérez-Peña, J.V., 2010. Human-driven coastline changes in the Adra River deltaic system, southeast Spain. Geomorphology, 119 (1), 9-22. 10.1016/j.geomorph.2010.02.004

Jabaloy-Sánchez, A., Lobo, F.J., Azor, A., Martín-Rosales, W., Pérez-Peña, J.V., Bárcenas, P., Macías, J., Fernández-Salas, L.M., Vázquez-Vílchez, M., 2014. Six thousand years of coastline evolution in the Guadalfeo deltaic system (southern Iberian Peninsula). Geomorphology, 206, 374-391. https://doi.org/10.1016/j.geomorph.2013.08.037

Kitheka, J.U., Obiero, M., Nthenge, P., 2005. River discharge, sediment transport and exchange in the Tana estuary, Kenya. Estuar. Coast. Shelf S., 63, 455-468. 10.1016/j.ecss.2004.11.011

Knighton, D., 1998. Fluvial forms and processes. New-York, Wiley and Sons, 383 pp.

Kondolf, G.M., Gao, Y., Annandale, G.W., Morris, G.L., Jiang, E., Zhang, J., Cao, Y., Carling, P., Fu, K., Guo, Q., Hotchkiss, R., Peteuil, C., Sumi, T., Wang, H-W, Wang, Z., Wei, Z., Wu, B., Wu, C., Yang,

C.T., 2014. Sustainable sediment management in reservoirs and regulated rivers: Experiences from five continents. Earth's Future, 2, 256-280.

Kuenzer, C., Ottinger, M., Liu, G., Sun, B., Baumhauer, R., Dech, S., 2014. Earth observation-based coastal zone monitoring of the Yellow River Delta: Dynamics in China's second largest oil producing region over four decades. Appl. Geogr., 55, 92–107. ISSN 01436228. https://doi.org/10.1016/j.apgeog.2014.08.015.

LCWRP, 1993. Louisiana Coastal Wetlands Restoration Plan. Retrieved of June 2, 2014, from: http://lacoast.gov/rfeports/cwcrp/1993/1993lcwrp-1executive_summary.pdf

Lehner, B., Liermann, C.R., Revenga, C., Vörösmarty, C., Fekete, B., Crouzet, P., Döll, P., Endejan, M., Frenken, K., Magome, J., Nilsson, C., Robertson, J.C., Rödel, R., Sindorf, N., Wisser, D., 2011. High-resolution mapping of the world's reservoirs and dams for sustainable river-flow management. Frontiers in Ecology and the Environment, 9, 494-502. https://doi.org/10.1890/100125

Liquete, C., Arnau, P., Canals, M., Colas, S., 2005. Mediterranean river systems of Andalusia, southern Spain, and associated deltas: a source to sink approach. Mar. Geol., 222-223, 471-495. https://doi.org/10.1016/j.margeo.2005.06.033

Lisitzin, A.P., 1972. Sedimentation in the world ocean: Soc. Econ. Paleont. Mineral. Spec. Pub. 17, 218 p.

Maillet, G., Vella, C., Berné, S., Friend, P.L., Amos, C.L., Fleury, T.J., Normand, A., 2006. Morphological changes and sedimentary processes induced by the December 2003 flood event at the present mouth of the Grand Rhône River (southern France). Mar. Geol., 234 (1-4), 159–177. ISSN 00253227. https://doi.org/10.1016/j.margeo.2006.09.025.

Malini, B.H., Nageswara Rao, K., 2004. Coastal erosion and habitat loss along the Godavari delta front a fallout of dam construction. Curr. Sci., 87 (9), 1232–1236.

Martins, O., Probst, J.-L., 1991. Biogeochemistry of major African rivers: carbon and mineral transport, in Degens, E.T., Kempe, S., Richey J.E. (Eds.), Biogeochemistry of Major World Rivers, SCOPE-42: Chichester, Wiley, 127-155.

Meade, R.H., Yuzyk, T.R., Day, T.J., 1990. Movement and storage of sediment in rivers of the United States and Canada: in Wolman, M.G., Riggs, H.C. (Eds.), The Geology of North America, vol. 1, Surface Water Hydrology: Boulder, Geol. Soc. America, 255-280.

Meybeck, M., Laroche, L., Durr, H.H. Syvitski, J.P.M., 2003. Global variability of daily total suspended solids and their fluxes in rivers, Glob. Planet. Change, 39, 65–93. https://doi.org/10.1016/S0921-8181(03)00018-3

Meybeck M, Ragu A, 1996. River discharges to the oceans: an assessment of suspended solids, major ions and nutrient. UNEP, Environment Information and Assessment: 240 pp.

Milliman, J.D., Farnsworth, K.L., 2011. River Discharge to the Coastal Ocean: A Global Synthesis. Cambridge University Press, Cambridge, 392 pp. ASIN B005253EIS

Milliman, J.D., Meade, R.H., 1983. World-wide delivery of river sediment to the oceans: Jour. Geology, 91, 1-21.

Moftakhari, H.R., Jay, D.A., Talke, S.A., Schoellhamer D.H., 2015. Estimation of historic flows and sediment loads to San Francisco Bay,1849–2011. J. Hydro., 529 (3), 1247-1261. 10.1016/j.jhydrol.2015.08.043

Moran, C., Prosser, I., De Rose, R., Lu, H., Croke, B., Hughes, A., Olley, J., Cannon, G., 2005. Sediments and nutrients in the rivers of the Murray-Darling Basin, Targeting the Future. Murray-Darling Basin Commission, Knowledge Series 14/05, MDBC, Canberra, 23 pp. ISBN 1921038462

Morgan, J.P., Larimore, P.B., 1957. Changes in the Louisiana shoreline. Technical Report Professional Paper, Coastal Studies Institute, Gulf Coast Association of Geological Societies Transactions, Louisiana State University, 7, 303–310.

Morgan, J.P., Morgan, D.J., 1957. Accelerating retreat rates along Louisiana's coast: Baton Rouge. Technical Report Professional Paper, Louisiana State University, 41 pp.

Morton, R.A., Miller, T.L., Moore, L.J., 2004. National Assessment of Shoreline Change: Part 1 Historical Shoreline Changes And Associated Coastal Land Loss Along The U. S. Gulf Of Mexico. Technical report, USGS numbered series 2004-1043, Geological Survey (U.S.), Center for Coastal and Watershed Studies, 44 pp. https://doi.org/10.3133/ofr20041043.

Morton, R.A., Pieper, M.J., 1975. Shoreline Changes in the Vicinity of the Brazos River Delta (San Luis Pass to Brown Cedar Cut), an Analysis of Historical Changes of the Texas Gulf Shoreline. Technical Report 4, University of Texas, GC7504, 47 pp. ISSN: 0082-3309.

Morton, R.A., Speed, F.M., 1998. Evaluation of Shorelines and Legal Boundaries Controlled by Water Levels on Sandy Beaches. J. Coastal Res., 14 (4), 1373–1384. ISSN 07490208, 15515036. http://www.jstor.org/stable/4298899.

Muñoz-Salina, E., Castillo, M., 2015. Streamflow and sediment load assessment from 1950 to 2006 in the Usumacinta and Grijalva Rivers (Southern Mexico) and the influence of ENSO. Catena, 127, 270-278. https://doi.org/10.1016/j.catena.2015.01.007

Murali, R.M., Shrivastava, D., Vethamony, P., 2009. Monitoring shoreline environment of Paradip, east coast of India using remote sensing. Curr. Sci. India, 97 (1), 79-84.

Nageswara Rao, K., Subraelu, P., Naga Kumar, K., Demudu, G., Hema Malini, B., Rajawat, A., Ajai, 2010. Impacts of sediment retention by dams on delta shoreline recession: evidences from the Krishna and Godavari deltas, India. Earth Surf. Proc. Land., 35, 817–827. ISSN 01979337. https://doi.org/10.1002/esp.1977.

Nageswara Rao, K., Saito, Y., Nagakumar, K., Demudu, G., Rajawat, A.S., Kubo, S., Li, Z., 2015. Palaeogeography and evolution of the Godavari delta, east coast of India during the Holocene: An example of wave-dominated and fan-delta settings. Palaeogeogr. Palaeoclim., Palaeoeco., 440, 213–233. ISSN 0031-0182. https://doi.org/10.1016/j.palaeo.2015.09.006.

Nienhuis, J.H., Ashton, A.D., Giosan, L., 2015. What makes a delta wave-dominated? Geology, 43 (6), 511–514. https://doi.org/10.1130/G36518.1.

Nkounkou, R.R., Probst, J.L., 1987. Hydrology and geochemistry of the Congo River system. In: Degens, E.T., Kempe, S., Weibin, G. (Eds.), Transport of Carbon and Minerals in Major World Rivers, Part 4. Mitt. Geol-Paläont. Inst. Univ. Hamburg, SCOPE/UNEP Sond., 64, 483-508.

Obowu, C.D., Abam, T.K.S., 2014. Spatial and Multi-Temporal Change Analysis of the Niger Delta Coastline Using Remote Sensing and Geographic Information System (GIS). Int. J. Remote Sens. Appl., 4 (1), 41–47. ISSN 2226-4353. https://doi.org/10.14355/ijrsa.2014.0401.04.

Ollivier, P., Hamelin, B., Radakovitch, O., 2010. Seasonal variations of physical and chemical erosion: A three-year survey of the Rhone River (France). Geochim. Cosmochim. Acta 74 (3), 907–927. https://doi.org/10.1016/j.gca.2009.10.037

OSR, 2016. Bilan actualisé des flux particulaires du Rhône Action III.3 Version du 13 juillet 2016 – Bilan actualisé des flux de matières en suspension et micropolluants associés sur le bassin du Rhône pour la période 2011-2015 - Rapport d'avancement - Poulier, G.

Overeem, I., Syvitski, J.P.M., 2009. Dynamics and Vulnerability of Delta Systems. Technical Report 35, LOICZ Reports & Studies, GKSS Research Center, Geesthacht, 54 pp.

Paine, J.G., Mathew, S., Caudle, T., John, A., Jackson, K.G., 2011. Texas Gulf Shoreline Change Rates through 2007. Technical Report 10, Bureau of Economic Geology, GCAGS Journal, 1, 13–26.

Palanques, A., Plana, F., Maldonado, A., 1990. Recent influence of man on the Ebro margin sediment system, northwestern Mediterranean Sea: Marine Geol., 95, 247-263. https://doi.org/10.1016/0025-3227(90)90119-5

Pekel, J.-F., Cottam, A., Gorelick, N., Belward, A.S., 2016. High-resolution mapping of global surface water and its long-term changes. Nature, 540 (7633), 418–422. ISSN 0028-0836. http://dx.doi.org/10.1038/nature20584.

Penland, S. (Project coordinator), 1996. Historical shoreline change in the north gulf of Mexico. Technical Report Professional Paper, US Environmental Protection Agency, Gulf of Mexico Program, map scale 1:2,000,000.

Penland, S., Kulp, M.A., 2005. Deltas, In: Schwartz, M. (Ed.), Encyclopedia of Coastal Science, Springer, Dordrecht, 362–368. ISBN 978-1-4020-1903-6.

Penland, S., Connor, P.F., Cretini, F., Westphal, K., 2003. CWPPRA adaptive management: assessment of five barrier island restoration projects in Louisiana. Electronic proceed. Coast. Sed., 70148 (504), 12 pp.

Preoteasa L, Vespremeanu-Stroe A, Tătui F, Zăinescu F, Gabor-Timar A, Cârdan I. 2016. The evolution of an asymmetric deltaic lobe (Sf. Gheorghe, Danube) in association with cyclic development of the river-mouth bar: Long-term pattern and present adaptations to human-induced sediment depletion. Geomorphology, 253: 59–73. https://doi.org/10.1016/j.geomorph.2015.09.023

Priest, G.R., 1999. Coastal shoreline change study: Northern and Central Lincoln County, Oregon. J. Coastal Res., 140–157. ISSN 07490208, 15515036. http://www.jstor.org/stable/25736192.

Ramesh, R., Subramanian, V., 1988. Temporal, spatial and size variation in the sediment transport in the Krishna River Basin. Jour. Hydrol., 98, 53-65.

Rand McNally, 1980. Encyclopedia of World Rivers. London: Bison Books Limited, 350.

Ronco, P., Fasolato, G., Nones, M., Di Silvio, G., 2010. Morphological effects of damming on lower Zambezi River. Geomorphology, 115, 43-55,

Rooney, J., Fletcher, C., Barbee, M., Eversole, D., Lim, S.-C., Richmond, B., Gibbs, A., 2003. Dynamics of sandy shorelines in Maui, Hawaii - SOEST Hawaii: Consequences and causes. In: Davis, R.A., Sallenger, A., Howd. P. (Eds.), Coastal Sediments 03–Crossing Disciplinary Boundaries: Proceedings of the International Conference on Coastal Sediments. Clearwater Beach, Florida ASCE. 3, 1–14.

Rooseboom, A., von M. Harmse, H.J., 1979. Changes in the sediment load of the Orange River during the period 1929-1969. Int. Assoc. Hydrol. Sci. Pub. 128, 459-470.

Ruddiman, W.F., 2003. The anthropogenic greenhouse era began thousands of years ago. Climatic Change, 61 (3), 261–293. ISSN 1573-1480. https://doi.org/10.1023/B:CLIM.0000004577.17928.fa.

Saito, Y., Yang, Z., Hori, K., 2001. The Huanghe (Yellow river) and Changjiang (Yangtze river) deltas: A review on their characteristics, evolution and sediment discharge during the Holocene. Geomorphology, 41, 219–231. https://doi.org/10.1016/S0169-555X(01)00118-0.

Salomon, L.N., 2005. Géomorphologie sous-marine et littorale. Presses Universitaires de Bordeaux: Pessac, 285–290. ISBN 2867815223/978-2867815225.

Seijger, C., Douven, W. van Halsema, G., Hermans, L., Evers, J., Phi, H.L., Khan, M.F., Brunner, J., Pols, L., Ligtvoet, W., Koole, S., Slager, K., Vermoolen, M.S., Hasan, S., Hoang, V.T., 2016. An analytical framework for strategic delta planning: negotiating consent for long-term sustainable delta development. J. Environ. Manage. 60 (8), 1485-1509. https://doi.org/10.1080/09640568.2016.1231667

Sestini, G., 1992. Implications of climatic changes for the Nile Delta. In Jeftic, L., Milliman, J.D., Sestini G. (Eds.), Edward Arnold Publ, UK, 535-601.

Shaw, J. B., Wolinsky, M.A., Paola, C., Voller, V.R., 2008. An image-based method for shoreline mapping on complex coasts. Geophys. Res.Lett., 35, L12405, doi:10.1029/2008GL033963.

Simms, A.R., Rodriguez, A.B., Anderson, J.B., 2018. Bayhead deltas and shorelines: Insights from modern and ancient examples. Sedimentary Geology, 374, 17-35. https://doi.org/10.1016/j.sedgeo.2018.07.004

Sliti, M., 1990. Fonctionnement des brise-lames dans le système littoral du golfe de Tunis [Dissertation]. Bordeaux I University I: 444.

Snoussi, M., Haida, S., Imassi, S., 2002. Effects of the construction of dams on the Moulouya and the Sebou rivers (Morocco). Reg Environ Change, 3: 5–12. https://doi.org/10.1007/s10113-001-0035-7

Smith, S.E., Abdel-Kader, A., 1988. Coastal Erosion Along the Egyptian Delta. J. Coastal Res., 4 (2), 245–255. http://www.jstor.org/stable/4297400.

SOBA. Ayeyarwady State of the Basin Assessment. WWF Greater Mekong, 2017.

Suanez, S., Provansal, M., 1996. Morphosedimentary behaviour of the deltaic fringe in comparison to the relative sea-level rise on the Rhône delta. Quat. Sci. Rev., 15 (96), 811–818. https://doi.org/0217-3191/96.

Syvitski, J.P.M., 2008. Deltas at risk. Sustain. Sci., 3 (1), 23–32. ISSN 1862-4057. https://doi.org/10.1007/s11625-008-0043-3.

Syvitski, J.P.M., Kettner, A.J., Overeem, I., Hutton, E.W.H., Hannon, M.T., Brakenridge, G.R., Day, J., Vörösmarty, C., Saito, Y., Giosan, L., Nicholls, R.J., 2009. sinking deltas due to human activities. Nat. Geosci., 2 (10), 681–686. ISSN 1752-0894. https://doi.org/10.1038/ngeo629.

Syvitski, J.P., Morehead, M.D., 1999. Estimating river-sediment discharge to the ocean: application to the eel margin, northern California. Mar. Geol., 154, 13–28. https://doi.org/10.1016/ S0025-3227(98)00100-5.

Syvitski, J.P.M., Morehead, M., Nicholson, M., 1998a. Hydrotrend: a climate-driven hydrologic-transport model for predicting discharge and sediment load to lakes or oceans. Comput. Geosci., 21, 51–68. https://doi.org/10.1016/S0098-3004(97)00083-6.

Syvitski, J.P.M., Nicholson, M., Skene, K., Morehead, M., 1998b. Plume 1.1: deposition of sediment from a fluvial plume. Comput. Geosci., 24:159–171. https://doi.org/10.1016/S0098-3004(97) 00084-8.

Syvitski, J.P.M., Saito, Y., 2007. Morphodynamics of deltas under the influence of humans. Glob. Planet. Chang., 57, 261–282. https://doi.org/10.1016/j.gloplacha.2006.12.001.

Syvitski, J.P.M., Vörösmarty, C.J., Kettner, A.J., Green, P., 2005. Impact of humans on the flux of terrestrial sediment to the global coastal ocean. Science, 308, 376–380. 10.1126/science.1109454

Tessler, Z.D., Vorosmarty, C.J., Grossberg, M., Gladkova, I., Aizenman, H., Syvitski, J.P.M., Foufoula-Georgiou, E., 2015. Profiling risk and sustainability in coastal deltas of the world. Science, 349, 638-643.

Tessler, Z. D., Vörösmarty, C. J., Overeem, I., and Syvitski, J. P. M., 2018. A model of water and sediment balance as determinants of relative sea level rise in contemporary and future deltas. Geomorphology, 305, 209-220. https://doi.org/10.1016/j.geomorph.2017.09.040

Thanh, T.D., Saito, Y., Huy, D.V., Cu, N.H., Chien, D.D., 2005. Coastal erosion in Red River delta: current status and response, In: Chen, Z., Saito, Y., Goodbred Jr, S.L. (Eds.), Mega-Deltas of Asia: Geological Evolution and Human Impact, China Ocean Press, Beijin, 98–106. ISBN 7-5027-6432-2/P-863.

Thao, N.V., 2008. Mapping land-use/cover and detecting the landuse/cover changes in the coast of Red River Delta by using remotely sensed data and GIS technology, Project report reserved at the Institute of Marine Environment and Resources, 18–23.

Thieler, R.E., Himmelstoss, E.A., Zichichi, J.L., Ergul, A., 2017. The digital shoreline analysis system (DSAS) version 4.0, an ArcGIS extension for calculating shoreline change (ver. 4.4, july 2017). U.S. Geological Survey Open-File Report. 2008–1278.

Tixeront, J., 1960. Débit solide des cours d'eau en Algérie et en Tunisie. IAHS Publ., 53: 26–42.

Torab, M., Azab, M., 2006. Modern shoreline changes along the Nile delta coast as an impact of construction of the Aswan high dam. Geogr. Techn., 2, 69–76.

Trépanier, I., Dubois, J.-M.M., Bonn, F., 2002. Suivi de l'évolution du trait de côte à partir d'images HRV (XS) de SPOT: Application au delta du fleuve Rouge, Viêt-Nam. Int. J. Remote Sens., 23 (5), 917–937. https://doi.org/https://doi.org/10.1080/01431160110070348.

Uehara, K., Sojisuporn, P., Saito, Y., Jarupongsakul, T., 2010. Erosion and accretion processes in a muddy dissipative coast, the Chao Phraya River delta, Thailand. Earth Surf. Proc. Land., 35, 701–1711. https://doi.org/10.1002/esp.2012.

UNESCO/IAHS. 1966. Gross Sediment Transport into Oceans, First Preliminary Edition. UNESCO/IAHS, Paris. AVS/NR/IHD/III/05, WS/1066/99/AVS, 11 pp. https://unesdoc.unesco.org/ark:/48223/pf0000142096

UNEP, 1982. River inputs to the west and central African marine environment: UNEP Regional Seas Reports and Studies No. 5, 62 pp.

Van Beek, J., Meyer-Arendt, K., 1982. Louisiana's eroding coastline: Recommendations for protection. Technical Report Professional Paper, Louisiana Department of Natural Resources, 49 pp. ASIN B0006Y48GM.

Van Maren, B., 2004. Morphodynamics of a cyclic prograding delta: The Red River, Vietnam. Dissertation, University Utrecht, Nederlandse Geografische Studies, 324, 167 p.

Vericat, D., Batalla, R.J., 2006. Sediment transport in a large impounded river: The lower Ebro, NE Iberian Peninsula, Geomorphology, 79 (1–2), 72–92. 15 September.

Vespremeanu-Stroe, A., Tătui, F., Constantinescu, Ş., Zăinescu, F., 2017. Danube delta coastline evolution (1856–2010), in: Rădoane, M., Vespremeanu-Stroe, A., (Eds.), Landform Dynamics and Evolution in Romania, Springer International Publishing, pp. 551-564

Walling, D.E., Fang, D., 2003. Recent trends in the suspended sediment loads of the world's rivers. Glob. Planet. Change, 39, 111–126.

Wang, H., Yang, Z., Saito, Y., Liu, J.P., Sun, X., Wang, Y., 2007. Stepwise decreases of the Huanghe (Yellow River) sediment load (1950-2005): Impacts of climate change and human activities. Glob. Planet. Chang., 57 (3), 331–354. ISSN 0921-8181. https://doi.org/10.1016/j.gloplacha.2007.01.003.

Wang, C., Zhao, Y., Zou, X., Xu, X., Ge, C., 2017. Recent changing patterns of the Changjiang (Yangtze River) Estuary caused by human activities. Acta Oceanologica Sinica, 36 (4), 87-96. 10.1007/s13131-017-1017-z

WLE, 2017. Dataset on the Dams of the Irrawaddy, Mekong, Red and Salween River Basins. https://wle-mekong.cgiar.org/maps/.

Wu, Z.Y., Saito, Y., Zhao, D.N., Zhou, J.Q., Cao, Z.Y., Li, S.J., Shang, J.H., Liang, Y.Y., 2016. Impact of human activities on subaqueous topographic change in Lingding bay of the Pearl river estuary, china, during 1955 – 2013. Sci. Rep., 6, 219–231. https://doi.org/10.1038/srep37742.

Zamora-Arroyo, F., Nelson, S.M., Flessa, K.W., Nomura, R., 2013. Post-dam sediment dynamics and processes in the Colorado River estuary: Implications for habitat restoration, Ecological Engineering, 59, 134-143.

Zamora-Arroyo, F., Flessa, K.W., 2009. Nature's fair share: finding and allocating water for the Colorado River delta. In: Lopez Hoffman, L.L., McGovern, E.D., Varady, R., Flessa, K.W. (Eds.), Conservation of shared environments: Learning from the United States and Mexico. University of Arizona Press, Tucson, Arizona, USA, 23-38.

Zhang, W., Mu, S., Zhang, Y., Chen, K., 2011. Temporal variation of suspended sediment load in the Pearl River due to human activities. Int. J. Sed. Res., 26 (4), 487-497. https://doi.org/10.1016/S1001-6279(12)60007-9

Zhu, C., Zhang, X., Huang, Q., 2018. Four decades of estuarine wetland changes in the Yellow River delta based on Landsat observations between 1973 and 2013. Water, 10 (7), 933. https://doi.org/10.3390/w10070933

| Deltas | References for shoreline change analysis | Period covered in the literature | This study |
|---|---|---|---|
| Adra | Jabaloy-Sánchez et al. (2010) | 1956 – 2002 | 2002 – 2015 |
| Amazon | - | - | 1984 – 2015 |
| Arno | Bini et al. (2008); Besset et al. (2017) | 1938 - 2015 | - |
| Ayeyarwady | Hedley et al. (2010) | 1925 - 2006 | 1974 – 2015 |
| Brazos | Morton and Pieper (1975); Paine et al. (2011) | 1853 - 2001 | 2001 – 2015 |
| Burdekin | - | - | 1974 – 2015 |
| Ceyhan-Seyhan | Besset et al. (2017) | 1984 -2015 | - |
| Chang Jiang | Chu et al. (2013); Wang et al. (2017) | 1974 - 2014 | - |
| Chao Phraya | Uehara et al. (2010) | 1969 - 2001 | 1996 – 2015 |
| Colorado (Mx) | - | - | 1989 – 2015 |
| Colorado (Tx) | Morton and Pieper (1975); Paine et al. (2011) | 1856 - 2007 | 2005 – 2015 |
| Colville | - | - | 1985 – 2015 |
| Congo | - | - | 1989 – 2015 |
| Cunene | - | - | 1984 – 2015 |
| Danube | Vespremeanu-Stroe et al. (2017); Besset et al. (2017) | 1978 - 2014 | - |
| Dneiper | - | - | 1984 – 2014 |
| Ebro | Besset et al. (2017) | 1985 - 2015 | - |
| Fly | - | - | 1989 – 2015 |
| Ganges-Brahmaputra | Allison (1998) | 1792 - 1984 | 1972 – 2015 |
| Godavari | Malini and Nageswara Rao (2004); Nageswara Rao et al. (2010); Nageswara Rao et al. (2015) | 1930 - 2012 | 2008 – 2015 |
| Grijalva | - | - | 1986 – 2015 |
| Guadalfeo | Bergillos et al. (2016) | 1999 - 2014 | - |
| Indus | - | - | 1979 – 2015 |
| Krishna | Anand Rao et al. (2006) | 1920 - 2008 | 2008 – 2015 |
| Limpopo | - | - | 1979 – 2015 |
| Mackenzie | Salomon (2005); Hese and Overduin (2014) | 1950 - 2013 | - |
| Magdalena | - | - | 1973 – 2015 |
| Magra | - | - | 1984 – 2015 |
| Mahanadi | Murali et al. (2009) | 1972 - 2005 | 2005 – 2015 |
| Mangoky | - | - | 1973 – 2015 |

| River | Reference | Years | Years |
|---|---|---|---|
| Medjerda | Besset et al. (2017) | 1972 - 2015 | - |
| Mekong | Anthony et al. (2015) | 2003 - 2012 | 1972 – 2015 |
| Mississippi | Morgan and Larimore (1957); Adams et al. (1978); Van Beek and Meyer-Arendt (1982); Morgan and Morgan (1957); Penland (1996); Morton et al. (2004); Penland et al. (2003); Penland and Kulp (2005); Couvillion et al. (2011); Bentley et al. (2016) | 1850 - 2010 | 2010 – 2015 |
| Moulouya | Besset et al. (2017) | 1974 - 2015 | - |
| Murray | - | - | 1988 – 2015 |
| Niger | Adegoke et al. (2010); Obowu and Abam (2014); Dada et al. (2015); Kuenzer et al. (2014); Dada et al. (2018) | 1923 - 2013 | 1990 – 2015 |
| Nile | Smith and Abdel-Kader (1988); El-Fishawi (1989); Frihy et al. (1994); Fanos (1995); Torab and Azab (2006); Elsayed and Mahmoud (2007); Hereher (2011); Besset et al. (2017) | 1895 - 2015 | - |
| Ombrone | Cipriani et al. (2013) ; Besset et al. (2017) | 1954 - 2015 | - |
| Orange | - | - | 1984 – 2015 |
| Orinoco | - | - | 1986 – 2015 |
| Paraiba do Sol | - | - | 1976 – 2015 |
| Parana | - | - | 1995 – 2015 |
| Pearl | - | - | 1986 – 2015 |
| Po | Besset et al. (2017) | 1975 - 2015 | - |
| Red | Dien et al. (2003); Thanh et al. (2005); Thao et al. (2008) | 1930 - 2008 | 2008 – 2015 |
| Rhône | Suanez and Provansal (1996); Maillet et al. (2006) ; Besset et al. (2017) | 1823 - 2015 | - |
| Sao Francisco | - | - | 1985 – 2015 |
| Senegal | - | - | 1972 – 2015 |
| Shatt el Arab | - | - | |
| Tana | - | - | 1985 – 2015 |
| Vistula | Graniczny et al. (2004) | 1894 - 1997 | 1988 – 2015 |
| Volta | - | - | 1985 – 2015 |
| Yellow | Chu et al. (2006); Wang et al. (2007); Syvitski and Saito (2007); Chen et al. (2008); Bi et al. (2014); Zhu et al. (2018) | 1855 - 2013 | - |
| Zambezi | Ronco et al. (2010) | 1972 - 2004 | 1972 – 2015 |

| (a) Delta | $E_{AC}$ $(km^2/yr)$ | Delta | $E_{AC}$ $(km^2/yr)$ | Delta | $E_{AC}$ $(km^2/yr)$ |
|---|---|---|---|---|---|
| Amazon | 0.0092 | Guadalfeo | 0.0083 | Orange | 0.0093 |
| Adra | 0.009 | Yellow River | 0.0071 | Orinoco | 0.0099 |
| Arno | 0.0093 | Indus | 0.0078 | Paraiba do Sol | 0.0097 |
| Ayeyarwady | 0.0088 | Krishna | 0.0081 | Parana | 0.0094 |
| Brazos | 0.0091 | Limpopo | 0.0072 | Pearl | 0.0090 |
| Burdekin | 0.0085 | Mackenzie | 0.0089 | Red River | 0.0092 |
| Ceyhan-Seyhan | 0.0093 | Magdalena | 0.0085 | Po | 0.0099 |
| Chao Phraya | 0.0091 | Magra | 0.0098 | Rhône | 0.0061 |
| Colorado (Mx) | 0.0082 | Mahanadi | 0.0083 | Sao Francisco | 0.0092 |
| Colorado (Tx) | 0.0078 | Mangoky | 0.0074 | Senegal | 0.0086 |
| Colville | 0.0099 | Medjerda | 0.0076 | Shatt el Arab | 0.0079 |
| Cunene | 0.0093 | Mekong | 0.0088 | Tana | 0.0089 |
| Danube | 0.0078 | Mississippi | 0.0089 | Vistula | 0.0099 |
| Dneiper | 0.0092 | Moulouya | 0.0092 | Volta | 0.0079 |
| Ebro | 0.0088 | Murray | 0.0093 | Chang Jiang | 0.0086 |
| Fly | 0.0094 | Niger | 0.0095 | Congo | 0.0085 |
| Ganges-Brahmaputra | 0.0097 | Nile | 0.0098 | Zambezi | 0.0094 |
| Godavari | 0.0087 | Ombrone | 0.0090 | Grijalva | 0.0072 |

| (b) Kilometric indicator | | 1 | 2 | 3 | 4 | 5 | 6 | 7 | 8 | 9 |
|---|---|---|---|---|---|---|---|---|---|---|
| Surface error $(km^2)$ | $ShaE_{t_0}$ | 0.31 | 0.33 | 0.28 | 0.30 | 0.29 | 0.37 | 0.39 | 0.40 | 0.40 |
| | $ShaE_{t_1}$ | 0.01 | 0.03 | 0.05 | 0.03 | 0.03 | 0.03 | 0.03 | 0.06 | 0.06 |
| Quadratic error | $\delta_t$ | 0.31 | 0.33 | 0.29 | 0.30 | 0.30 | 0.37 | 0.39 | 0.41 | 0.40 |
| Dates | 1973 | 01/20/1973 | | | | | | | | |
| | 2014 | 01/01/2014 | | | | | | | | |
| Time interval (yr) | | 40.947 | | | | | | | | |
| $E_{AC}$ $(km^2/yr)$ | 1973-2014 | 0.008 | 0.008 | 0.007 | 0.007 | 0.007 | 0.009 | 0.01 | 0.010 | 0.01 |

| Delta | $E_{AC_{ACB}}$ (%) | Delta | $E_{AC_{ACB}}$ (%) | Delta | $E_{AC_{ACB}}$ (%) |
|---|---|---|---|---|---|
| Adra | 0.14 | Godavari | 0.26 | Ombrone | 0.11 |
| Amazon | 0.27 | Grijalva | 0.26 | Orange | 0.15 |
| Arno | 0.11 | Guadalfeo | 0.15 | Orinoco | 0.26 |
| Ayeyarwady | 0.20 | Indus | 0.22 | Paraiba do Sol | 0.20 |
| Brazos | 0.50 | Krishna | 0.22 | Parana | 0.16 |
| Burdekin | 0.30 | Limpopo | 0.07 | Pearl | 0.22 |
| Ceyhan-Seyhan | 0.18 | Mackenzie | 0.02 | Po | 0.15 |
| Chang Jiang | 0.18 | Magdalena | 0.22 | Red River | 0.29 |
| Chao Phraya | 0.25 | Magra | 0.06 | Rhone | 0.10 |
| Colorado (Mx) | 0.15 | Mahanadi | 0.20 | Sao Francisco | 0.20 |
| Colorado (Tx) | 0.17 | Mangoky | 0.19 | Senegal | 0.19 |
| Colville | 0.03 | Medjerda | 0.16 | Shatt el Arab | 0.17 |
| Cunene | 0.32 | Mekong | 0.25 | Tana | 0.35 |
| Danube | 0.11 | Mississippi | 0.39 | Vistula | 0.13 |
| Dneiper | 0.19 | Moulouya | 0.11 | Volta | 0.36 |
| Ebro | 0.14 | Murray | 0.26 | Yellow River | 0.13 |
| Fly | 0.06 | Niger | 0.28 | Congo | 0.21 |
| Ganges-Brahmaputra | 0.33 | Nile | 0.20 | Zambezi | 0.12 |

| River | Sediment load (kg/s) after 1970 | References for post-1970 sediment loads | References for pre-1970 sediment loads | GRDC database |
|---|---|---|---|---|
| Adra | 4.8 | Arjona et al., 2018 | Liquete et al., 2005 | - |
| Amazon | 38461 | Milliman and Farnsworth, 2011; Syvitski and Saito, 2007 | - | X |
| Arno | 72 | Billi and Rinaldi, 1997 | Holeman, 1968 | - |
| Ayeyarwady | 8377 | Milliman and Farnsworth, 2011; Syvitski and Saito, 2007 | - | X |
| Brazos | 308 | Milliman and Farnsworth, 2011; Syvitski and Saito, 2007 | Judson and Ritter, 1964 | X |
| Burdekin | 308 | Belperio, 1979 | - | X |
| Ceyhan | 180 | EIE, 1993; Çetin et al., 1999; Milliman and Farnsworth, 2011; Anthony et al., 2014 | Milliman and Farnsworth, 2011; Anthony et al., 2014 | X |
| Chang Jiang | 15867 | Milliman and Meade, 1983; Milliman and Farnsworth, 2011; Syvitski and Saito, 2007 | - | X |
| Chao Phraya | 355 | Milliman and Farnsworth, 2011; Syvitski and Saito, 2007 | - | X |
| Colorado (Mx) | 49 | Zamora-Arroyo and Flessa, 2009; Zamora-Arroyo et al., 2013 | Meybeck et al., 2003; Syvitski and Saito, 2007 | X |
| Colorado (Tx) | 3872 | Milliman and Farnsworth, 2011; Syvitski and Saito, 2007 | - | X |
| Colville | 49 | - | - | X |
| Cunene | 31 | Milliman and Farnsworth, 2011 | - | X |
| Danube | 2221 | Milliman et Farnsworth, 2011; Preoteasa et al., 2016 | Walling and Fan, 2003; Syvitski and Saito, 2007 | X |
| Dneiper | 34,23 | Hay, 1987 | - | X |
| Ebro | 647 | Palanques et al., 1990; Vericat and Batalla, 2006; Goudie and Viles, 2016 | Syvitski et al., 2005; Syvitski and Saito, 2007; Milliman and Farnsworth, 2011; Anthony et al., 2014; Goudie and Viles, 2016 | X |
| Fly | 2339 | Milliman and Farnsworth, 2011; Syvitski and Saito, 2007 | Harris, 1991 | - |
| Ganges-Brahmaputra | 35559 | Milliman and Farnsworth, 2011; Syvitski and Saito, 2007 | - | X |

| | | | | |
|---|---|---|---|---|
| Godavari | 5561 | Milliman and Farnsworth, 2011; Syvitski and Saito, 2007 | - | X |
| Grijalva | 10 | Muñoz-Salina and Castillo, 2015 | Muñoz-Salina and Castillo, 2015 | - |
| Guadalfeo | 2.7 | Jabaloy-Sanchez et al., 2014 | Liquete et al., 2005 | - |
| Indus | 7978 | Milliman and Farnsworth, 2011; Syvitski and Saito, 2007 | Milliman et al., 1987 | X |
| Krishna | 2246 | Milliman and Farnsworth, 2011; Syvitski and Saito, 2007 | Ramesh and Subramanian, 1988 | X |
| Limpopo | 1157 | Milliman and Farnsworth, 2011; Syvitski and Saito, 2007 | - | X |
| Mackenzie | 3273 | Milliman and Farnsworth, 2011; Syvitski and Saito, 2007; Meybeck and Thorne, 2003 | Syvitski, 1992 | X |
| Magdalena | 7156 | Milliman and Farnsworth, 2011; Syvitski and Saito, 2007 | Milliman and Meade, 1983 | - |
| Magra | 3 | Cappucci et al., 2015 | Cappucci et al., 2015 | - |
| Mahanadi | 1953 | Gupta et al., 2012 | Chakrapani and Subramanian, 1990 | - |
| Mangoky | 1374 | - | Chaperon et al., 1993 | X |
| Medjerda | 297 | Sliti, 1990; Rand McNally, 1980; Meybeck and Ragu, 1996; Milliman and Farnsworth, 2011 | Tixeront, 1960 | X |
| Mekong | 3176 | Milliman and Farnsworth, 2011, Syvitski and Saito, 2007 | - | X |
| Mississippi | 12702 | LCWRP, 1993; Heimann et al., 2011 | Meade et al., 1990 | X |
| Moulouya | 787 | Snoussi et al., 2002; Milliman and Farnsworth, 2011; Anthony et al., 2014 | Milliman and Syvitski, 1992; Milliman and Farnsworth, 2011; Anthony et al., 2014 | X |
| Murray | 2915 | De Rose et al., 2004; Moran et al., 2005 | - | X |
| Niger | 1374 | Milliman and Farnsworth, 2011; Syvitski and Saito, 2007 | - | X |
| Nile | 3876 | Syvitski and Saito, 2007; Milliman and Farnsworth, 2011; Anthony et al., 2014; Goudie and Viles, 2016 | Sestini, 1991; Milliman and Farnsworth, 2011; Anthony et al., 2014; Goudie and Viles, 2016 | X |

| | | | | |
|---|---|---|---|---|
| Ombrone | 249 | Frangipane and Paris, 1994; Syvitski et al., 2005; Milliman and Farnsworth, 2011; Anthony et al., 2014 | Milliman and Farnsworth, 2011; Anthony et al., 2014 | - |
| Orange | 2915 | Knighton, 1998; Milliman and Farnsworth, 2011; Syvitski and Saito, 2007; Goudie and Viles, 2016 | Rooseboom and Harmse, 1979; Goudie and Viles, 2016 | X |
| Orinoco | 5663 | Milliman and Farnsworth, 2011; Syvitski and Saito, 2007 | - | X |
| Paraiba do Sol | 561 | Milliman and Farnsworth, 2011 | - | X |
| Parana | 3055 | Milliman and Farnsworth, 2011; Syvitski and Saito, 2007 | Depetris and Lenardon, 1982 | X |
| Pearl | 708 | Zhang et al., 2011 | Milliman and Meade, 1983; Zhang et al., 2011 | X |
| Po | 561 | Idroser, 1994; Syvitski and Kettner, 2007 | Unesco/IAHS, 1966; Milliman and Farnsworth, 2011; Anthony et al., 2014 | X |
| Red | 1617 | Van Maren, 2004; Milliman and Farnsworth, 2011; Syvitski and Saito, 2007 | - | X |
| Rhône | 1906 | Milliman and Meade, 1983; Ollivier et al., 2010; Dumas et al., 2015; OSR, 2016 | Milliman and Meade, 1983; Milliman and Farnsworth, 2011; Anthony et al., 2014 | X |
| Sao Francisco | 730 | Moftakhari et al., 2015 | Depetris and Paolini, 1991; Milliman and Meade, 1983; Moftakhari et al., 2015 | X |
| Senegal | 85 | Martins and Probst, 1991 | - | X |
| Shatt el Arab | 1762 | Milliman and Farnsworth, 2011; Syvitski and Saito, 2007 | Al-Mulla and Al-Ali, 2015 | X |
| Tana | 216 | Kitheka et al., 2005 | Kitheka et al., 2005 | X |
| Vistula | 85 | Milliman and Farnsworth, 2011; Syvitski and Saito, 2007 | Lisitzin, 1972 | X |
| Volta | 456 | Goudie and Viles, 2016 | UNEP, 1982; Goudie and Viles, 2016 | X |

| | | | | |
|---|---|---|---|---|
| Yellow | 34861 | Milliman and Farnsworth, 2011; Syvitski and Saito, 2007 | Syvitski and Saito, 2007 | X |
| Congo | 1601 | Milliman and Farnsworth, 2011; Syvitski and Saito, 2007 | Milliman and Meade, 1983; Nkounkou and Probst, 1987 | X |
| Zambezi | 634 | Ronco et al., 2010 | Ronco et al., 2010 | X |

**Table captions:**

Table 1. Literature references with data on delta shoreline evolution.

Table 2. Uncertainties in coastal area change rates (EAC) in km²/yr for each delta (a), and an example of error calculations for a 9-km long sector of the Mekong delta shoreline (b).

Table 3. Uncertainties in percentage evolution of the area of the active coastal band ($EAC_{ACB}$).

Table 4. Post-1970 sediment loads of the 54 rivers culled from the literature and from the Global Runoff Data Centre (GRDC) database (https://www.bafg.de/GRDC/EN/Home/homepage_node.html). References for the pre-1970 sediment loads discussed in the text are included here.

**Figure captions:**

Figure 1: Global map showing the 54 river deltas reviewed in this study.

Figure 2. Examples of operator-identified shoreline traces of the Ebro delta. Shaded area shows the active coastal band (2 km-wide from the 2015 shoreline).

Figure 3: Schematic illustration showing various conversions of a deltaic coastal strip (from the shoreline to 2 km inland) from water to land, and vice versa. The data retrieved for the 2 km-wide coastal band and calculated for the 54 deltas are from Donchyts et al. (2016) and Pekel et al. (2016).

Figure 4. Number of dams with a reservoir retention capacity > 1 km$^3$ downstream of hydrometric stations (black bars), and the reservoir retention capacity (red dots) that was not taken into account in the study of variations in pre-1970 versus post-1970 sediment loads.

Figure 5. Active coastal band (ACB) area for deltas with ACB gains (a) or losses (d), area change per annum for deltas with gains (b) or losses (e), and percentage of area gained (c) or lost (f) over 30 years in relation to the ACB in 2015, together with error margins (green bars). Dashed red line separates large from small deltas (see section 3.1.3).

Figure 6. The relationship between area of the active coastal band (ACB) and rate of area change within the ACB: (a) deltas with advancing shorelines; (b) deltas with retreating shorelines. *1. Colorado (Tx); 2. Indus; 3. Godavari; 4. Colorado (Mx); 5. Mississippi; 6. Mangoky; 7. Fly; 8. Magdalena; 9. Krishna; 10. Medjerda; 11. Chao Phraya; 12. Brazos; 13. Mahanadi; 14. Volta; 15. Grijalva; 16. Burdekin; 17. Niger; 18. Nile; 19. Ceyhan-Seyhan; 20. Moulouya; 21. Limpopo; 22. Colville; 23. Mackenzie; 24. Ebro; 25. Dneiper; 26. Sao Francisco; 27. Guadalfeo; 28. Rhône; 29. Ombrone; 30. Cunene; 31. Arno; 32. Shatt el Arab; 33. Adra; 34. Magra; 35. Murray; 36. Po; 37. Danube; 38. Tana; 39. Congo; 40. Senegal; 41. Vistula; 42. Paraiba do Sol; 43. Mekong; 44. Ayeyarwady; 45. Orinoco; 46. Orange; 47. Amazon; 48.*

*Zambezi; 49. Ganges-Brahmaputra; 50. Yellow River; 51. Parana; 52. Red River; 53. Pearl; 54. Chang Jiang.*

Figure 7. Examples of annual spatial variations in ACB area in individual deltas.

Figure 8. Temporal variability of the rate of change [km²/yr] of the ACB for a selection of deltas, the associated linear regressions and their p-values. The p-values concern the raw data, and not the annual anomalies. Using the non-parametric Mann-Kendal test to detect trend in the time series (positive, negative or non-null), we consider that with the null hypothesis $H_0$ (p-value > α in black), a trend does not exist, whereas $H_1$ (p-value < α in red) indicates a trend in the time series.

Figure 9. Graphs showing ranking of loss of delta ACB area with regards to the size of the ACB. The graph on the left shows the percentage of loss in ACB area, over 30 years, of each significantly eroding delta. The graph on the right shows a comparison of small (red dots: ACB area ≤ 400 km$^2$) and large deltas (black dots: ACB area >400 km$^2$) in terms of shorelines in erosion, shorelines with no significant change, and shorelines in advance. *1. Colorado (Tx); 2. Indus; 3. Godavari; 4. Colorado (Mx); 5. Mississippi; 6. Mangoky; 7. Fly; 8. Magdalena; 9. Krishna; 10. Medjerda; 11. Chao Phraya; 12. Brazos; 13. Mahanadi; 14. Volta; 15. Grijalva; 16. Burdekin; 17. Niger; 18. Nile; 19. Ceyhan-Seyhan; 20. Moulouya; 21. Limpopo; 22. Colville; 23. Mackenzie; 24. Ebro; 25. Dneiper; 26. Sao Francisco; 27. Guadalfeo; 28. Rhone; 29. Ombrone.*

Figure 10. The four categories of coastal land/water and water/land conversions over a period of 30 years for the 54 deltas. The graph on the right shows change in delta ACB area over the same period.

Figure 11. Map and graph showing the percentages of loss of fluvial sediment load between the pre-1970 period and the period 1970-2014. The post-1970 sediment loads are shown in Table 4.

Figure 12. Graphs showing the relationship between ACB area and post-1970 river sediment loads: black dots represent large ACB (> 400 km²), and red dots small ACB (≤ 400 km²). *1. Colorado (Tx); 2. Indus; 3. Godavari; 4. Colorado (Mx); 5. Mississippi; 6. Mangoky; 7. Fly; 8. Magdalena; 9. Krishna; 10. Medjerda; 11. Chao Phraya; 12. Brazos; 13. Mahanadi; 14. Volta; 15. Grijalva; 16. Burdekin; 17. Niger; 18. Nile; 19. Ceyhan-Seyhan; 20. Moulouya; 21. Limpopo; 22. Colville; 23. Mackenzie; 24. Ebro; 25. Dneiper; 26. Sao Francisco; 27. Guadalfeo; 28. Rhône; 29. Ombrone; 30. Cunene; 31. Arno; 32. Shatt el Arab; 33. Adra; 34. Magra; 35. Murray; 36. Po; 37. Danube; 38. Tana; 39. Congo; 40. Senegal; 41. Vistula; 42. Paraiba do Sol; 43. Mekong; 44. Ayeyarwady; 45. Orinoco; 46. Orange; 47. Amazon; 48. Zambezi; 49. Ganges-Brahmaputra; 50. Yellow River; 51. Parana; 52. Red River; 53. Pearl; 54. Chang Jiang;*

Figure 13. Graphs summarizing (a) area change within the ACB, (b) fluvial sediment load, (c) change in fluvial sediment load after 1970, and (d) land/water conversion in the ACB.

Figure 14. Indicative ranking of delta vulnerability based on reduction of fluvial sediment load and shoreline mobility.

Figure 15. Maps showing: (a) the distribution of the 54 river deltas grouped by continent/region and as a function of shoreline mobility, and (b) the individual deltas depicted on the basis of the four vulnerability levels shown in Fig. 14.

Figure 16. Potential loss of river sediments if dams reach their maximum storage capacity.

Figure 1

**Dates of shorelines**
— 1985
— 1990
— 2000
— 2015
▨ Area of the active coastal band (2 km)

Figure 2

**1984**

Surface $A_1$ of land converted into seasonal water

Surface $A_2$ of land converted into permanent water

Surface $A_3$ of water area converted into permanent land

Surface $A_4$ of water area converted into seasonal land

Here, $A_1 + A_2 > A_3 + A_4$

**2015**
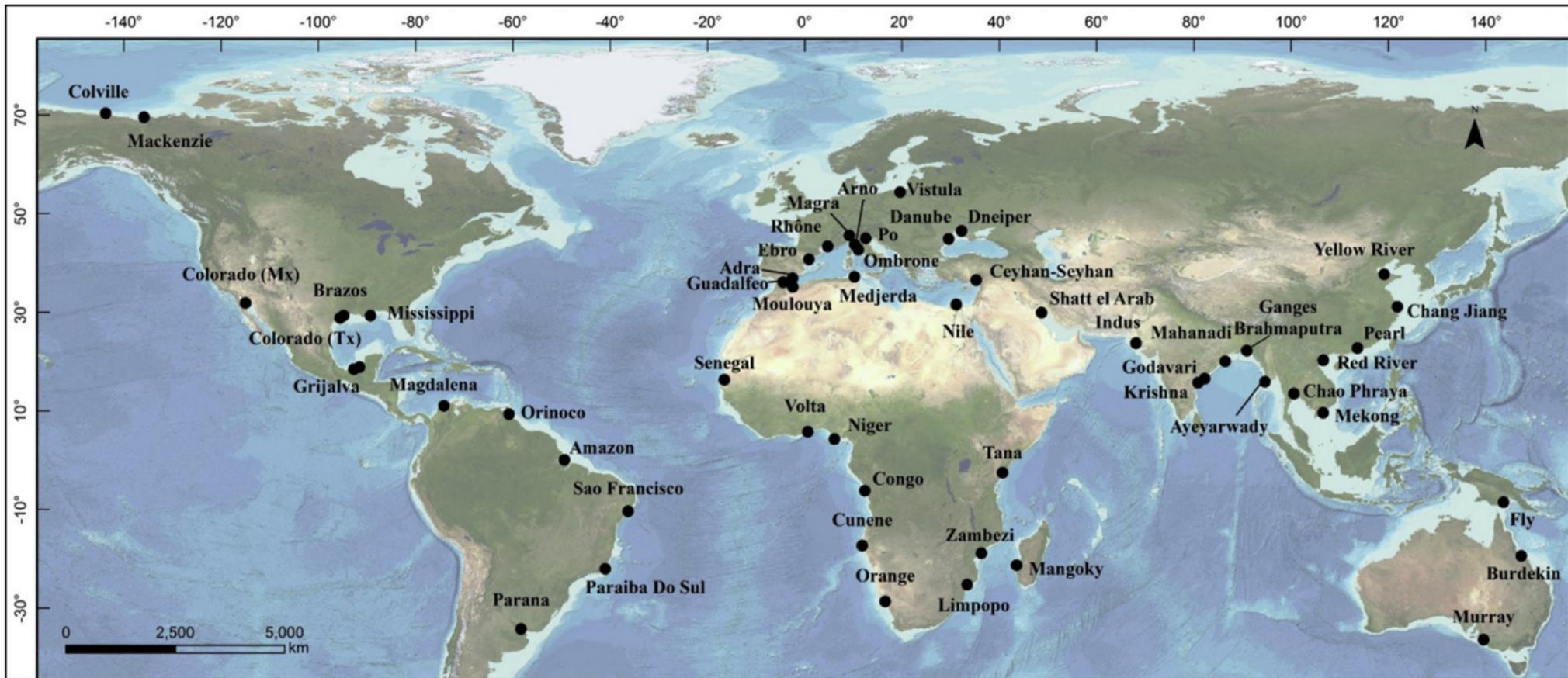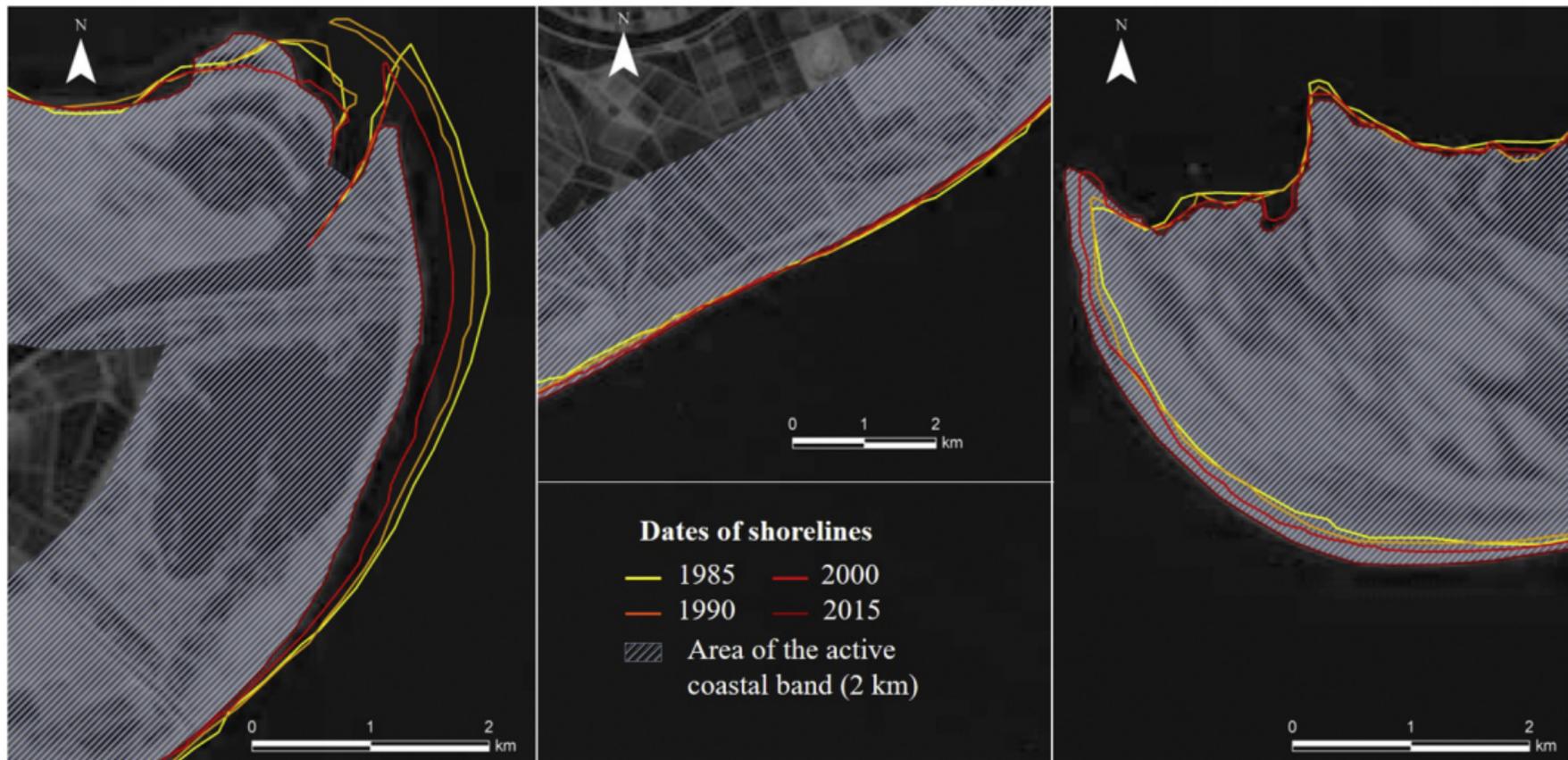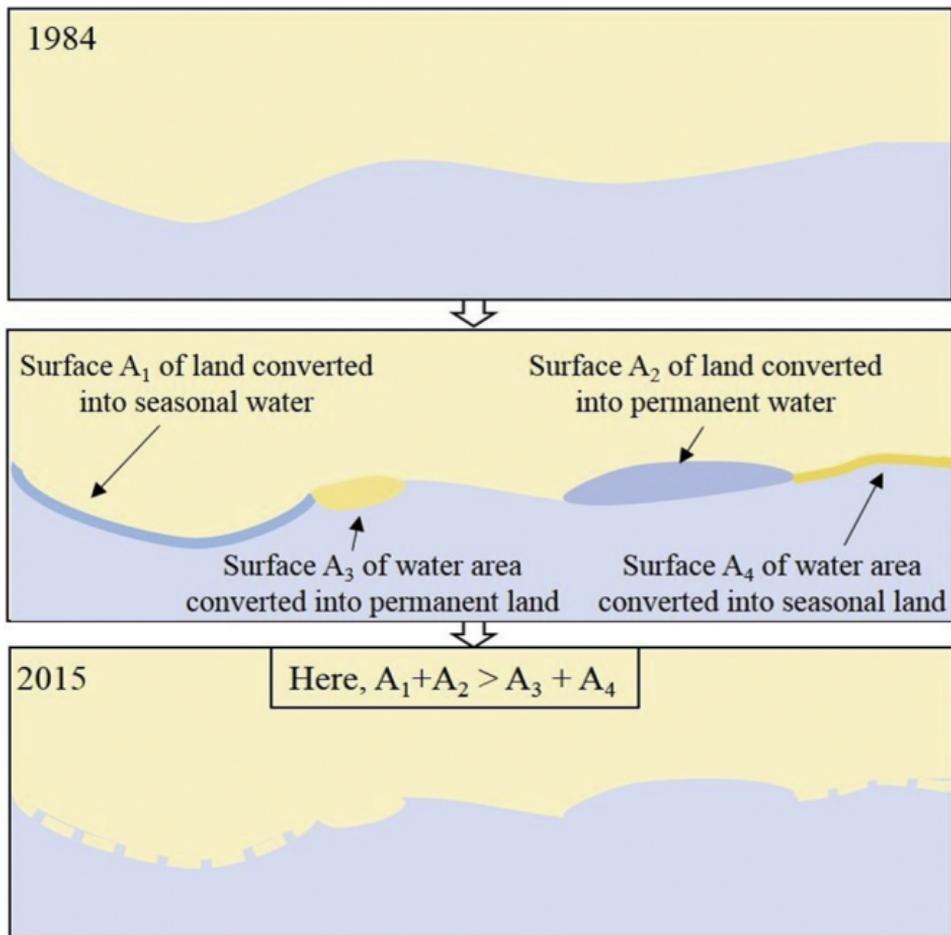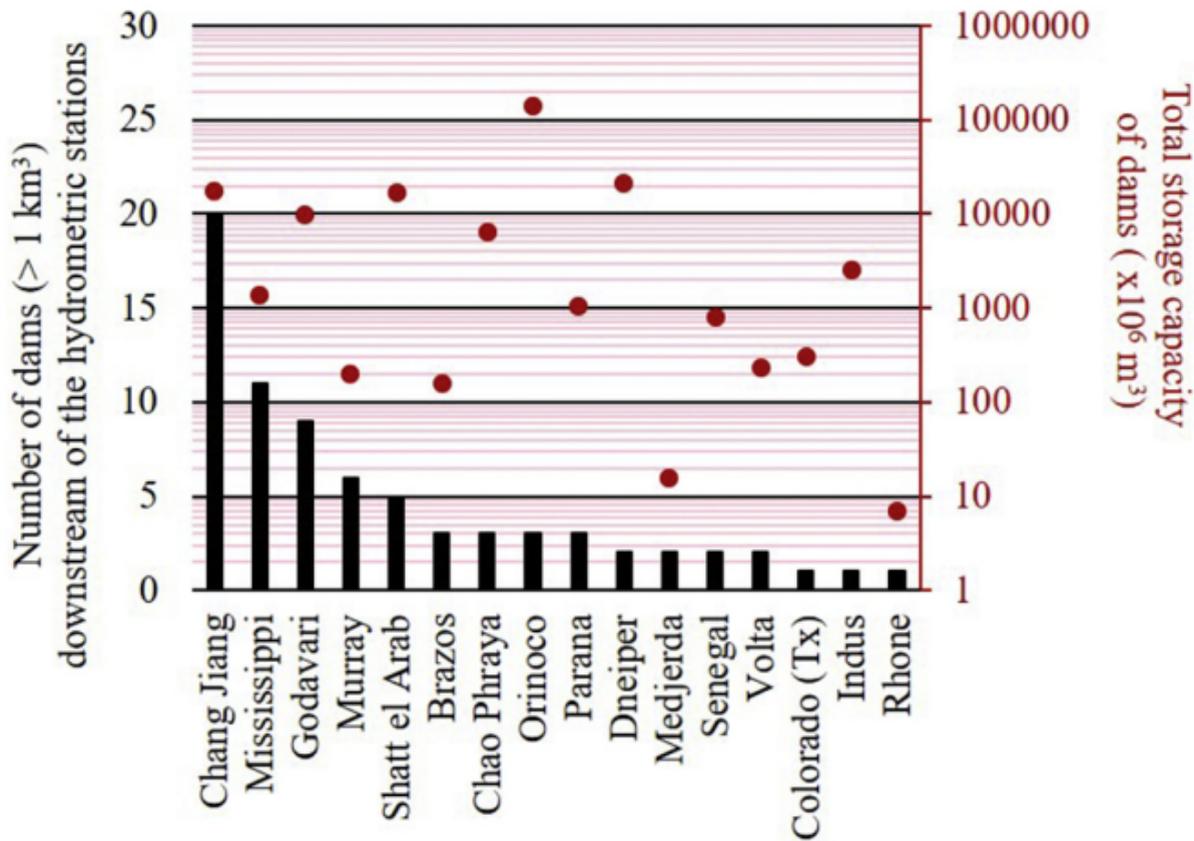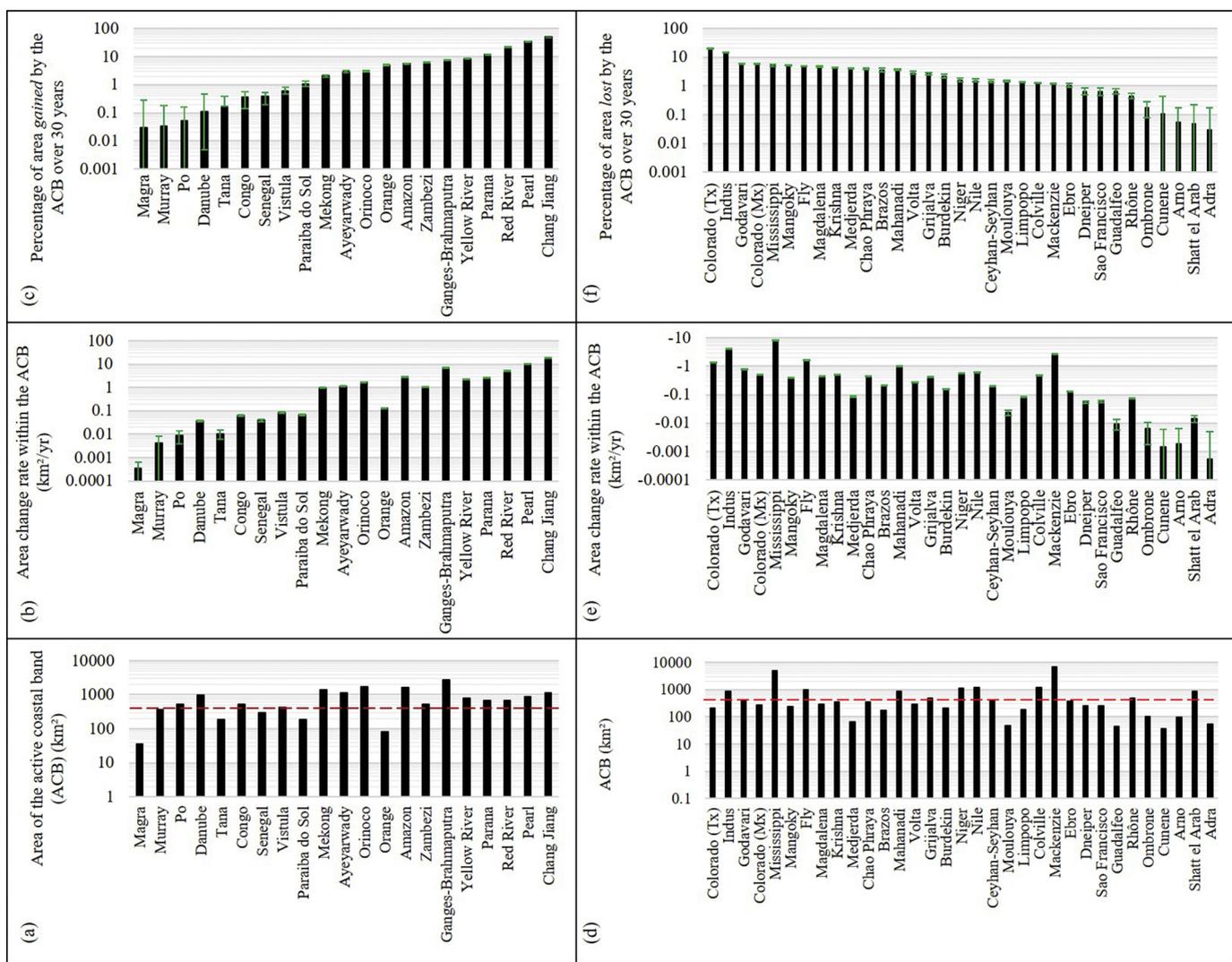
Figure 3

Figure 4

Figure 5
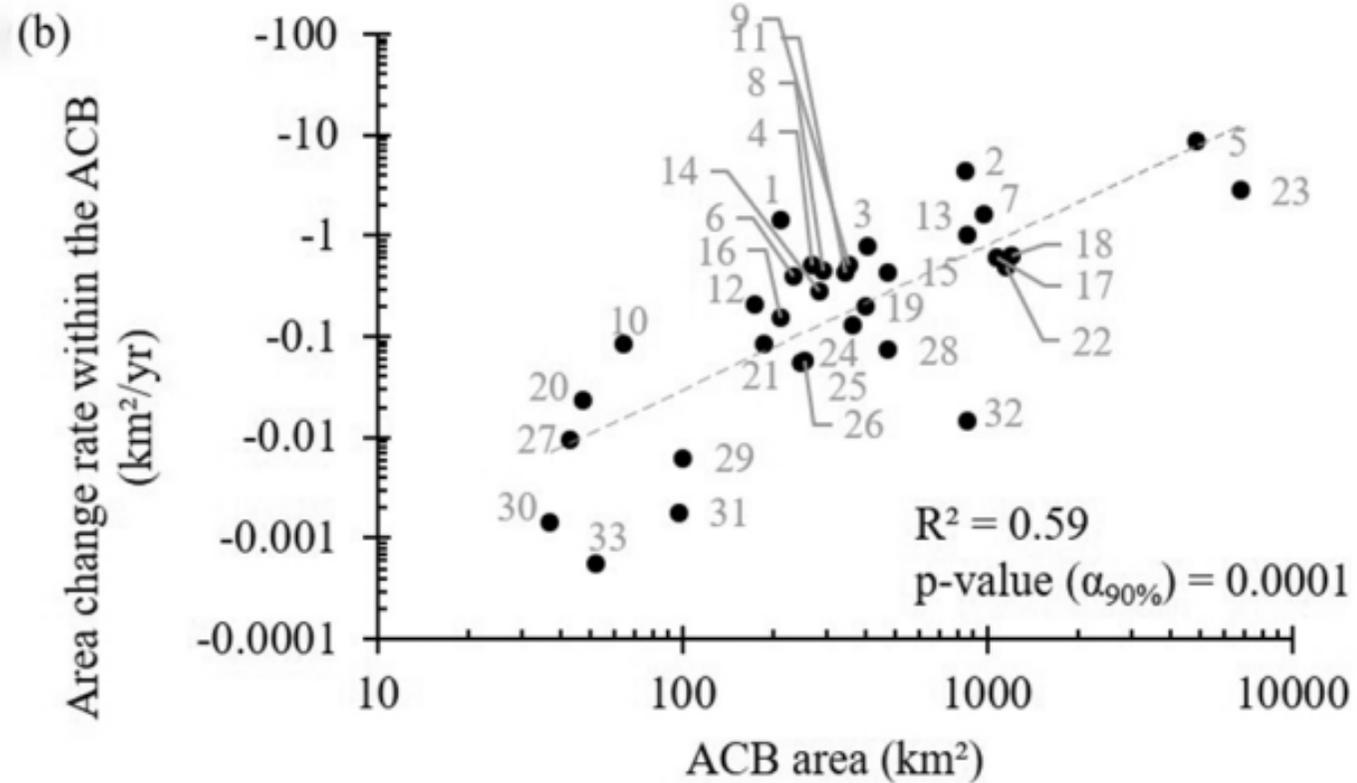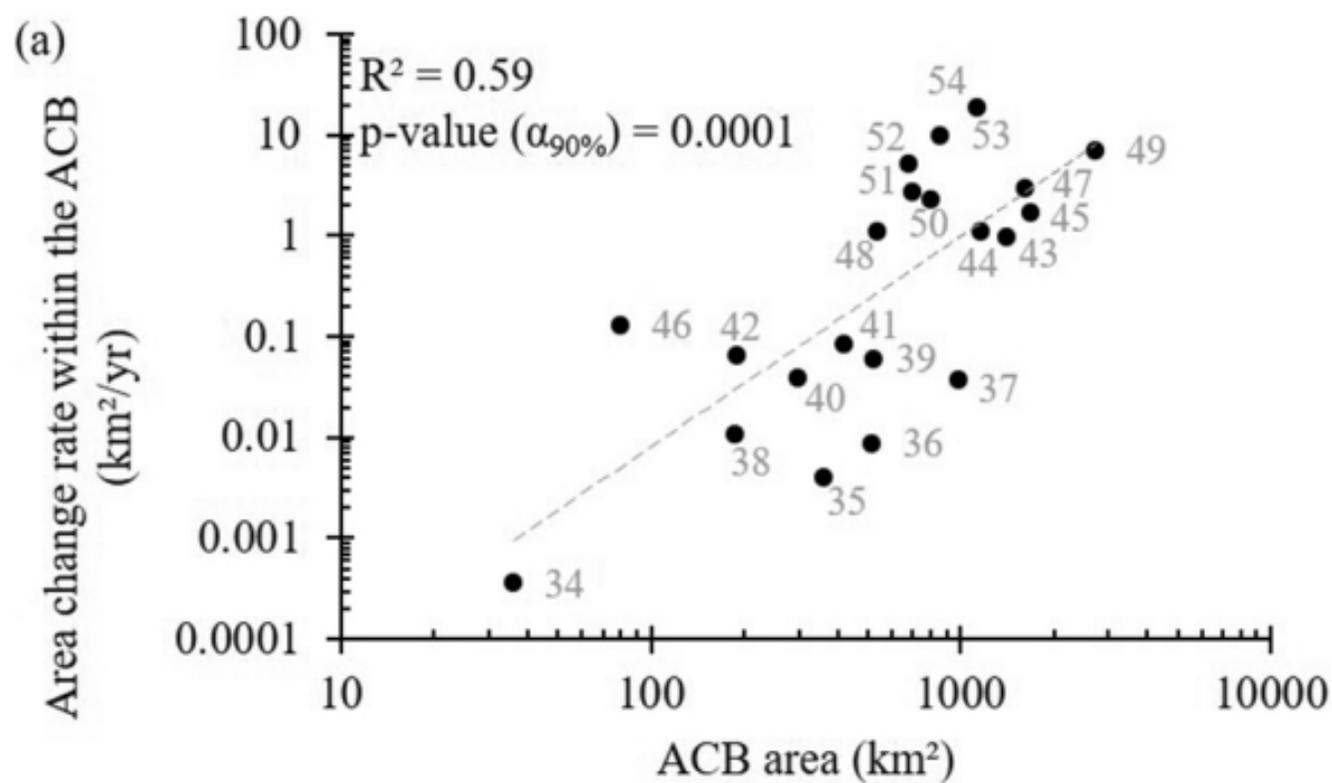
Figure 6
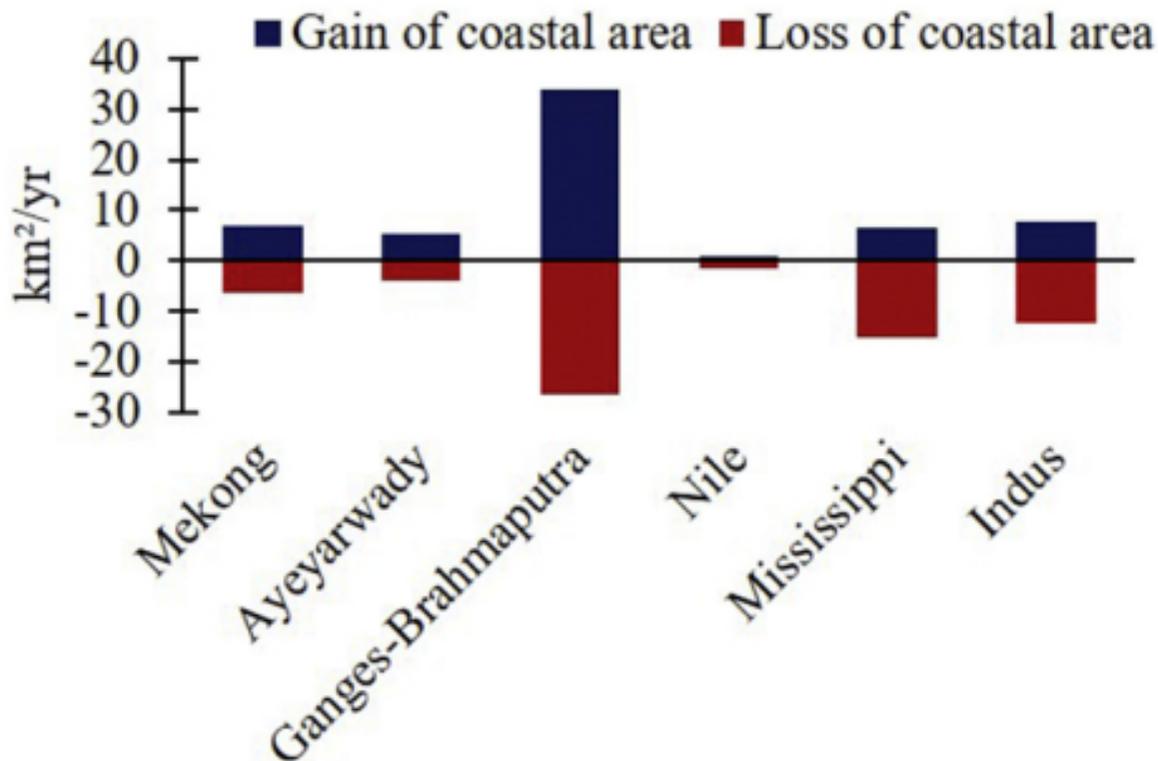
Figure 7
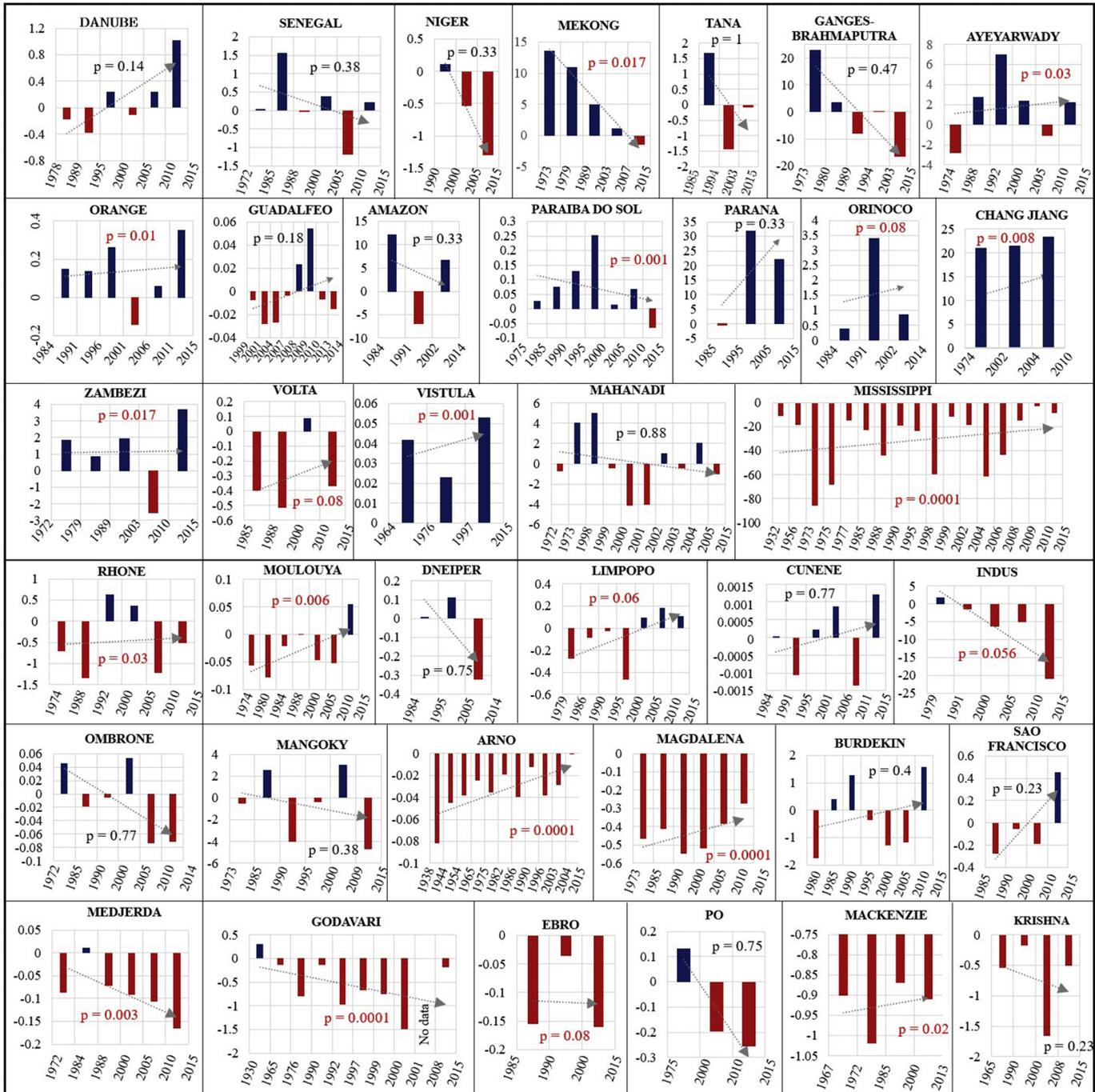
Figure 8
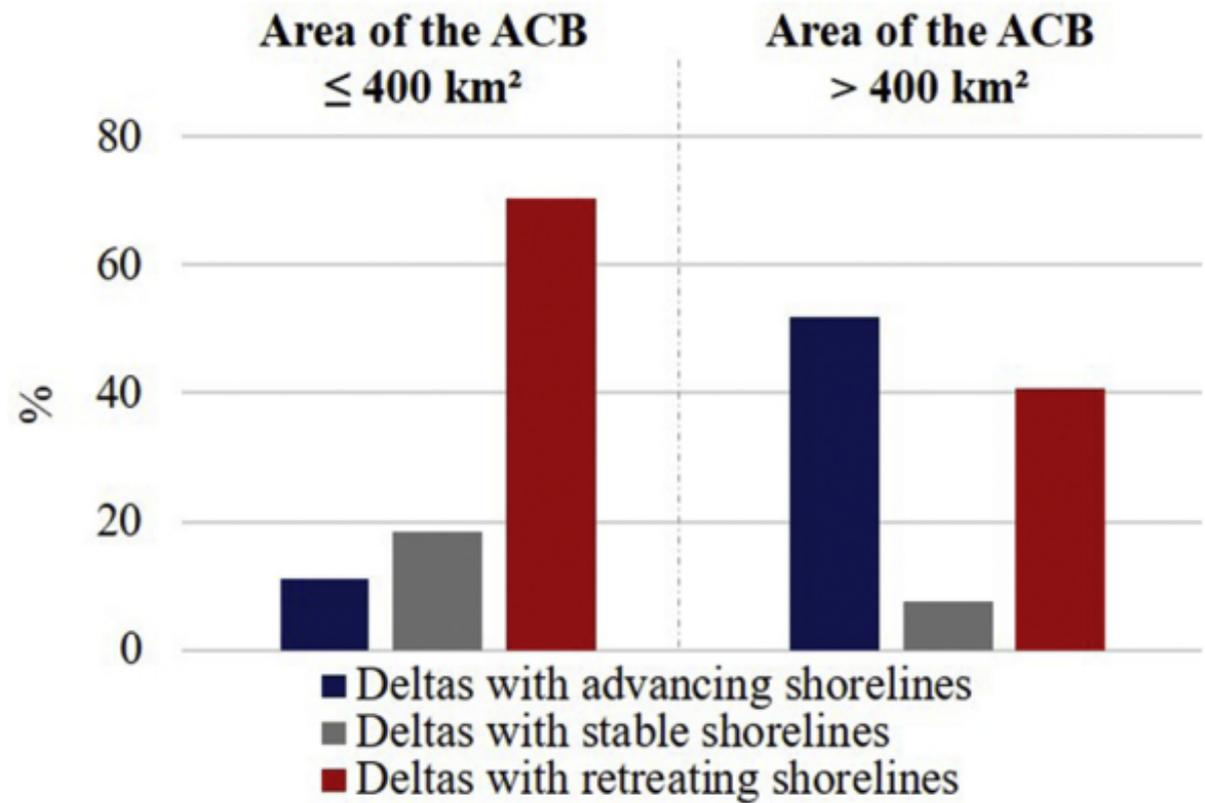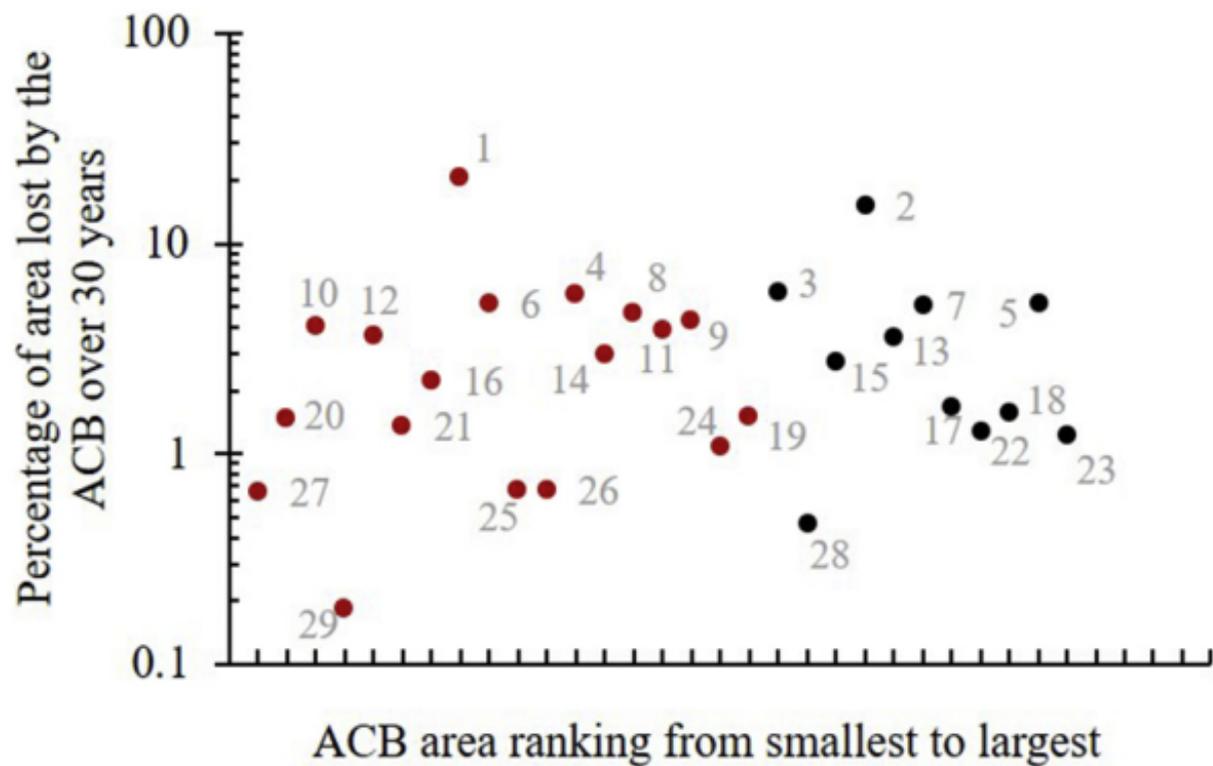
Figure 9
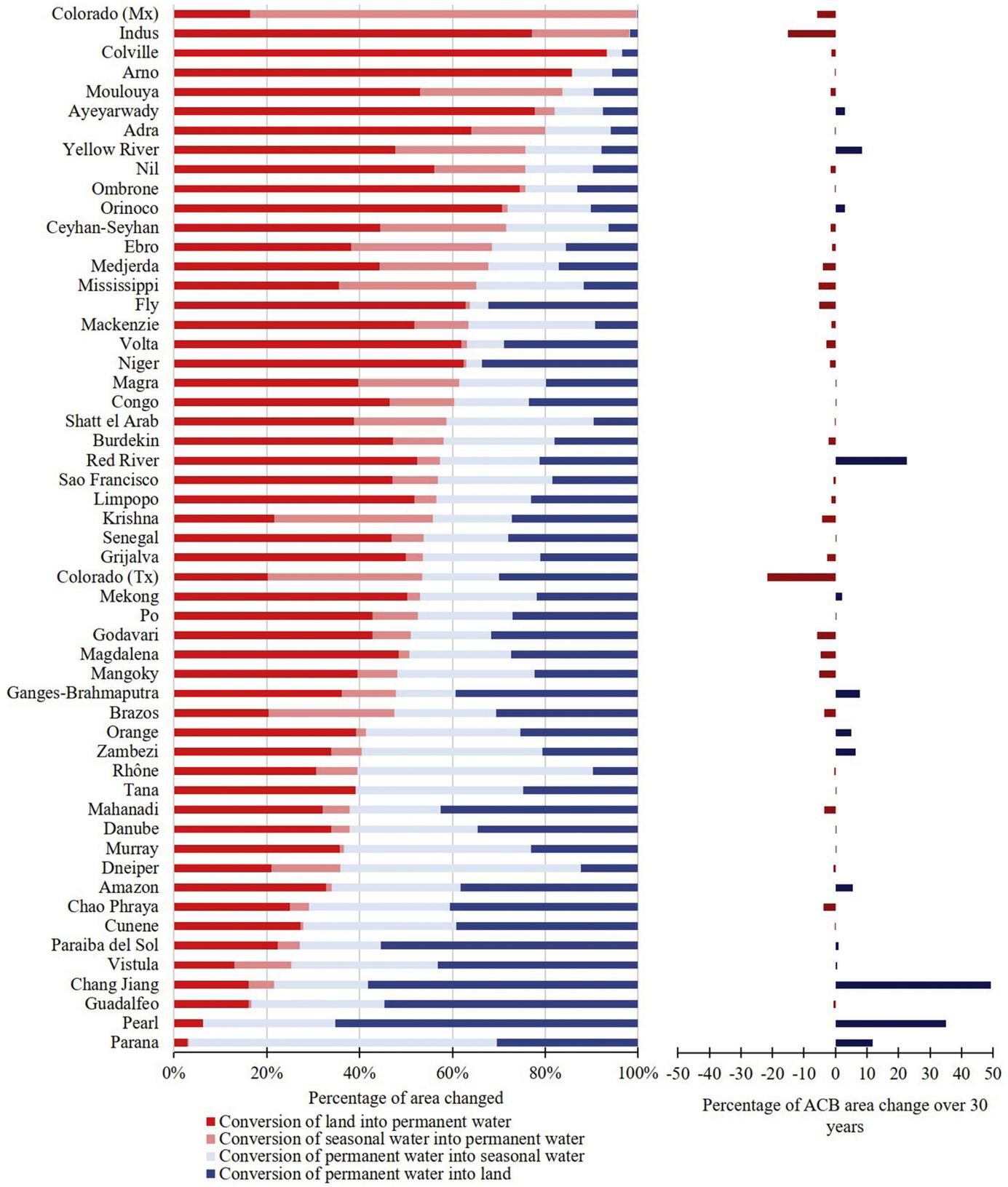
Figure 10
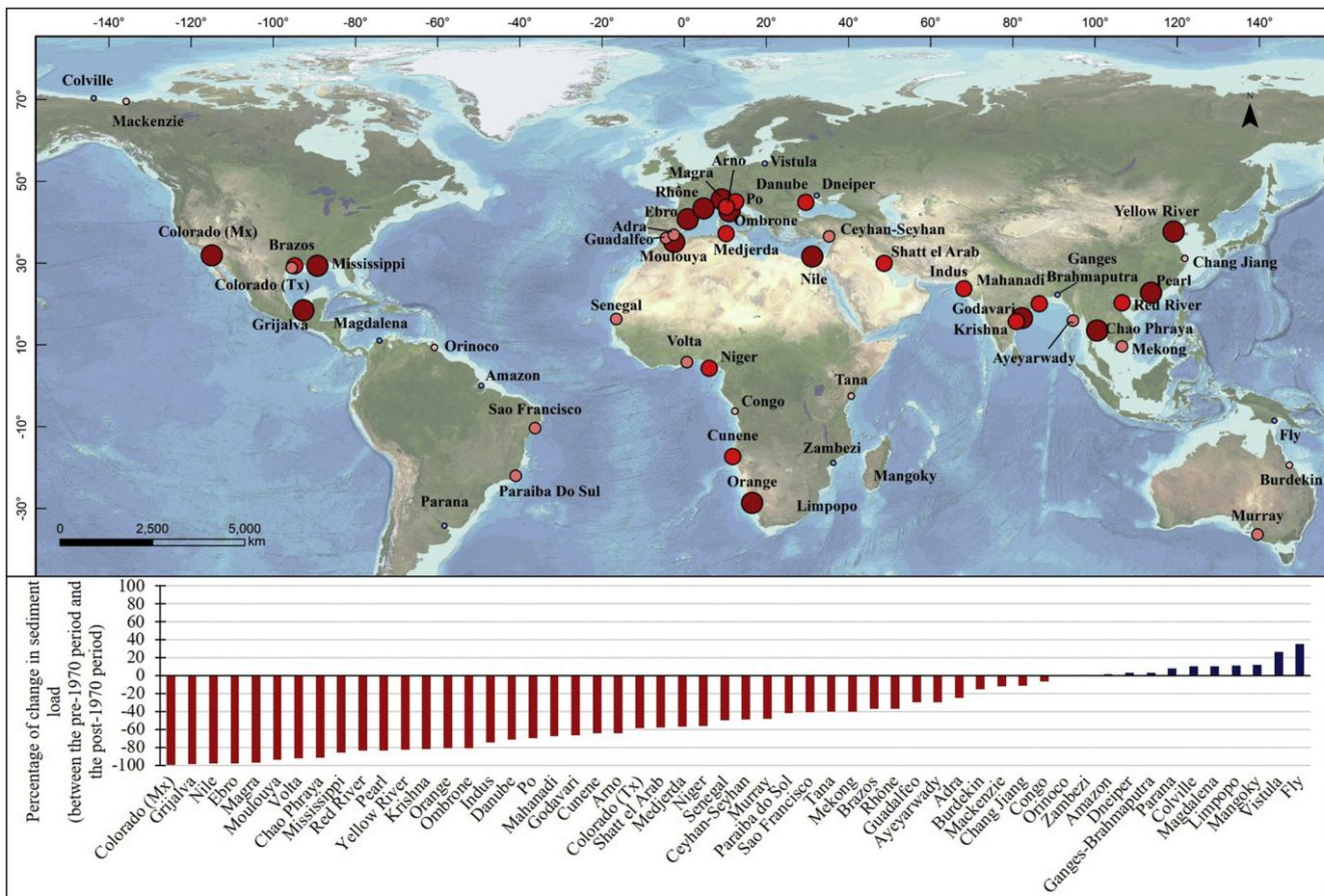
Figure 11
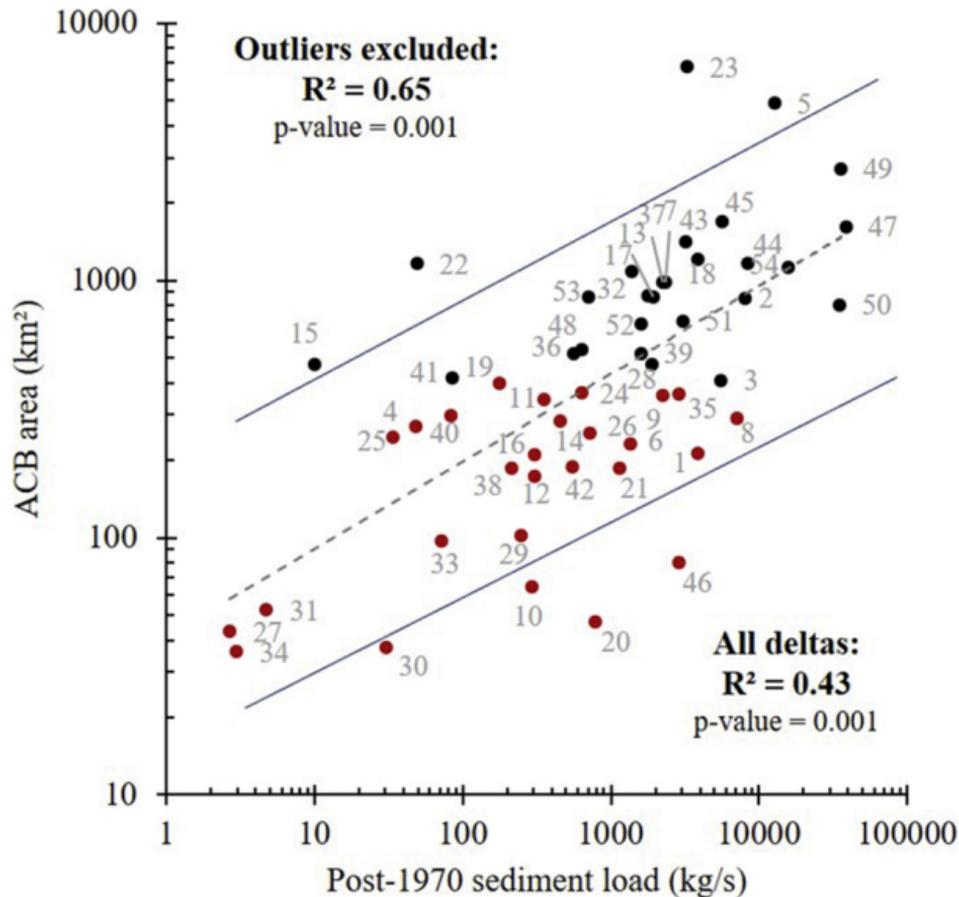
Figure 12
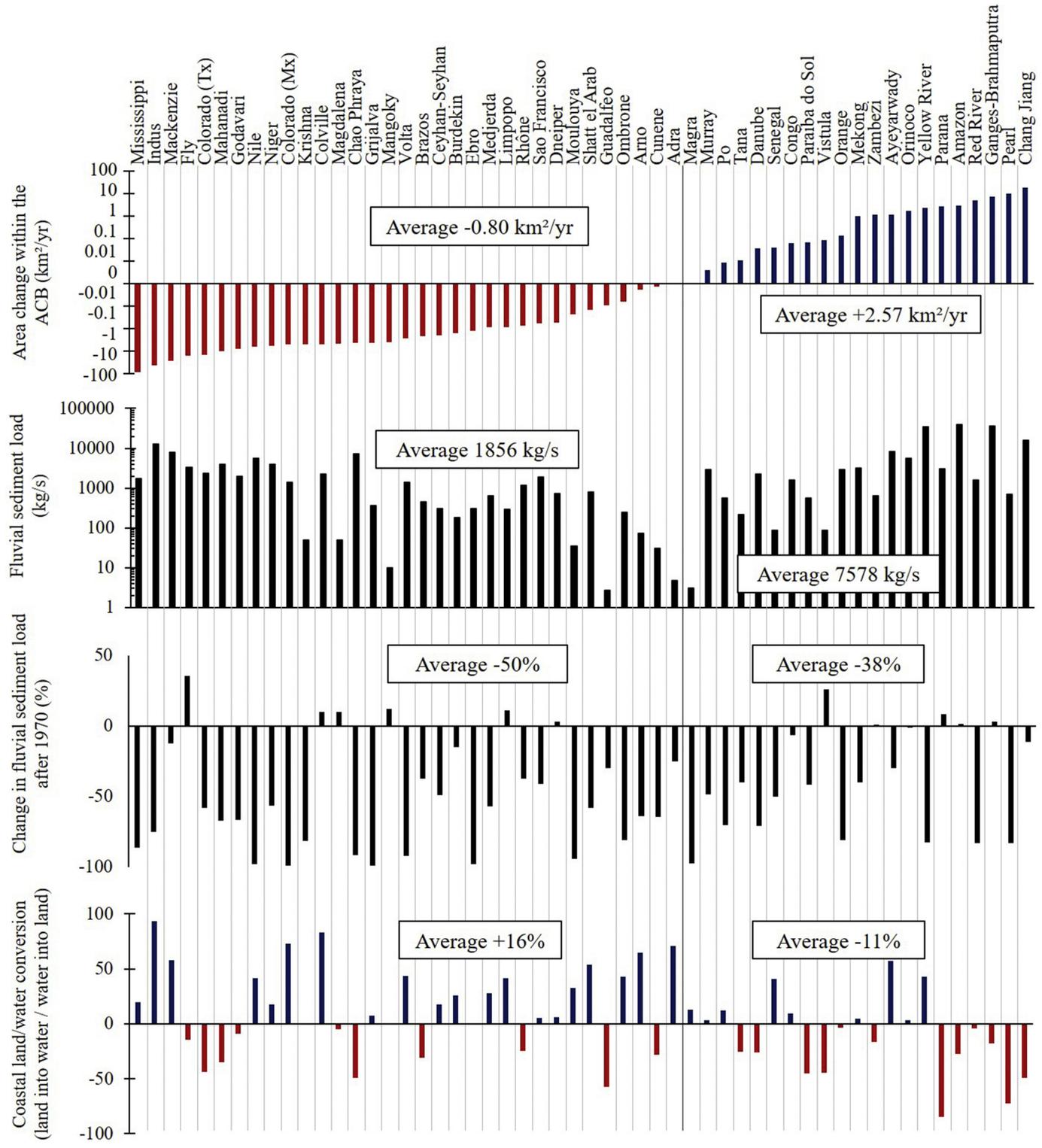
Figure 13

| Reduction of fluvial sediment load and level of relative delta vulnerability | | Multi-decadal shoreline mobility | Deltas |
|---|---|---|---|
| 4 (>50%) | Vulnerable | Retreat | Colorado (Mx), Nile, Ebro, Krishna, Indus, Mississippi, Colorado (Tx), Medjerda, Moulouya, Chao Phraya, Rhône, Ombrone, Mahanadi, Godavari, Niger |
| | | Stability | Cunene, Magra, Arno, Po |
| | | Advance | Yellow River, Orange, Danube, Red River, Pearl |
| 3 (<50%) | Vulnerable | Retreat | Brazos, Grijalva, Ceyhan-Seyhan, Sao Francisco, Volta, Guadalfeo |
| | | Stability | Murray, Adra, Shatt el Arab |
| | | Advance | Paraiba do Sol, Senegal, Ayeyarwady, Mekong |
| 2 (< 25%) | Vulnerable | Retreat | Mackenzie, Mangoky, Burdekin, Limpopo |
| | | Advance | Chang Jiang, Tana, Congo, Orinoco |
| 1 (No reduction) | Vulnerable | Retreat | Magdalena, Fly, Colville, Dneiper |
| | | Advance | Zambezi, Parana, Vistula, Amazon, Ganges-Brahmaputra |

Figure 14

Figure 15

Figure 16